UCSD/PTH 98-02
hep-ph/9803454
March 1998

Bottom Quark Mass from Υ Mesons

A.H. Hoang

Department of Physics, University of California, San Diego,
La Jolla, CA 92093–0319, USA

arXiv:hep-ph/9803454v1 26 Mar 1998

Abstract

The bottom quark pole mass M_b is determined using a sum rule which relates the masses and the electronic decay widths of the Υ mesons to large n moments of the vacuum polarization function calculated from nonrelativistic quantum chromodynamics. The complete set of next-to-next-to-leading order (i.e. $\mathcal{O}(\alpha_s^2, \alpha_s\, v, v^2)$ where v is the bottom quark c.m. velocity) corrections is calculated and leads to a considerable reduction of theoretical uncertainties compared to a pure next-to-leading order analysis. However, the theoretical uncertainties remain much larger than the experimental ones. For a two parameter fit for M_b, and the strong $\overline{\rm MS}$ coupling α_s, and using the scanning method to estimate theoretical uncertainties, the next-to-next-to-leading order analysis yields 4.74 GeV $\leq M_b \leq$ 4.87 GeV and $0.096 \leq \alpha_s(M_z) \leq 0.124$ if experimental uncertainties are included at the 95% confidence level and if two-loop running for α_s is employed. M_b and α_s have a sizeable positive correlation. For the running $\overline{\rm MS}$ bottom quark mass this leads to 4.09 GeV $\leq m_b(M_{\Upsilon(1S)}/2) \leq$ 4.32 GeV. If α_s is taken as an input, the result for the bottom quark pole mass reads 4.78 GeV $\leq M_b \leq$ 4.98 GeV (4.08 GeV $\leq m_b(M_{\Upsilon(1S)}/2) \leq$ 4.28 GeV) for $0.114 \lesssim \alpha_s(M_z) \leq 0.122$. The discrepancies between the results of three previous analyses on the same subject by Voloshin, Jamin and Pich, and Kühn *et al.* are clarified. A comprehensive review on the calculation of the heavy quark-antiquark pair production cross section through a vector current at next-to-next-to leading order in the nonrelativistic expansion is presented.

1 Introduction

Quantum chromodynamics (QCD) is the established theory of the strong interactions. The determination of its parameters, the strong coupling and the quark masses, and continuous tests of its consistency with experimental measurements belong to the most important tasks within particle physics. For the strong coupling an almost countless number of determinations exists. The most precise determinations now quote uncertainties in $\alpha_s(M_z)$ of less than 5%.[1] The remarkable feature of the α_s determinations, however, is their consistency to each other (see e.g. [1] for a review). The situation for the quark masses can certainly be described as much less coherent. For the bottom quark pole mass, which represents an important ingredient for the theoretical description of B mesons decays the determination of the corresponding Cabibbo-Kobayashi-Maskawa matrix elements, the situation is particularly confusing. In the past few years there have been three determinations by Voloshin ($M_b = 4.827 \pm 0.007$ GeV) [2], and later by Jamin and Pich ($M_b = 4.60 \pm 0.02$ GeV)[3] and Kühn *et al.* ($M_b = 4.75 \pm 0.04$ GeV) [4] which, although they have all been obtained from the same experimental data on the spectrum and the electronic decay widths of the Υ mesons, are contradictory to each other if the quoted uncertainties are taken seriously. Further, the three analyses [2, 3, 4] were all based on the same sum rule which relates large n moments (i.e. large number of derivatives at zero momentum transfer) of the vacuum correlator of two bottom-antibottom vector currents to an integral over the total production cross section of hadrons containing a bottom and an antibottom quark in e^+e^- annihilation. In the limit of large n the moments can be calculated in a nonrelativistic expansion [5, 6] and higher order (relativistic) corrections can be implemented in a systematic way.

This paper contains a determination of the bottom quark pole mass, where theoretical uncertainties are treated in a conservative way. It is partly motivated by the belief that a carefully performed analysis of theoretical uncertainties is mandatory in order to see whether the uncertainties presented in Refs. [2, 3, 4] are realistic. In this work the method of choice is to scan all theoretical parameters independently over reasonably large windows. We will show that this method to estimate theoretical uncertainties is more conservative than the methods used in Refs. [2, 3, 4]. In particular it renders the results obtained by Voloshin and Kühn *et al.* consistent to each other. With the scanning method the precise results of Voloshin and Kühn *et al.* can only be obtained if some model-like assumptions are imposed which are beyond first principles QCD. The by far bigger part of the motivation for this work, however, comes from the fact that now the technical and conceptual tools have been developed [7, 8, 9, 10] to include the next-to-next-to-leading order (NNLO) relativistic corrections to the large n moments into the analysis. A large fraction of this paper is devoted to a comprehensive presentation and review of the concepts and calculations necessary to determine those NNLO contributions. In particular, we use the concept of effective field theories formulated in the frame work of nonrelativistic quantum chromodynamics (NRQCD) [11, 12] to deal with the problems of ultraviolet divergences which arise if relativistic corrections to the expressions in the nonrelativistic limit are calculated. However, we regard NRQCD merely as a technical tool and do not spend too much time on formal considerations. Whenever possible we rely on physical rather than formal arguments and use results from older literature even if they have not been derived in the framework of NRQCD. It is the main intention of this work to calculate the NNLO corrections to the large n moments and to analyze their impact on the determination of M_b. We show that the NNLO corrections lead to a

[1] Throughout this paper the strong coupling is defined in the $\overline{\rm MS}$ scheme.

considerable reduction of theoretical uncertainties in the determination of M_b.

The program of this paper is as follows: In Section 2 we introduce our notation and explain the ideas and concepts on which our analysis and calculations are based on. NRQCD is introduced and a recipe for the calculation of the moments at NNLO is presented. Because the heavy quark-antiquark cross section in the threshold regime represents an important intermediate step in the calculation of the moments, Section 2 also contains a comprehensive review on the basic concepts involved in the calculation of the vector current induces cross section at NNLO. In Section 3 all calculations are carried out explicitly and all relevant formulae are displayed. Section 4 contains a discussion on some peculiarities of the large n moments. A detailed description of the treatment of the experimental data, the fitting procedure and the scanning method is given in Section 5. In Section 6 the numerical results are presented and discussed. Two different determinations of M_b are carried out. First, M_b and α_s are fitted simultaneously and, second, M_b is fitted while α_s is taken as in input. In Section 7, finally, we comment on the three previous analyses in Refs. [2, 3, 4] and Section 8 contains the conclusions. Attached to this paper are three appendices which contain material which we found too detailed to be presented in the main body of the paper.

The reader who is mainly interested in the results for the bottom quark mass can safely skip most of Section 2, and Sections 3 and 4 completely.

2 The Basic Ideas and Notation

The Sum Rule

We start our consideration from the correlator of two electromagnetic currents of bottom quarks at momentum transfer q

$$\Pi_{\mu\nu}(q) \;=\; -\,i \int \mathrm{d}x\, e^{i\,q.x}\, \langle\, 0 \,|\, T\, j^b_\mu(x)\, j^b_\nu(0) \,|\, 0 \,\rangle\,, \tag{1}$$

where

$$j^b_\mu(x) \;= \bar{b}(x)\, \gamma_\mu\, b(x)\,. \tag{2}$$

The symbol b denotes the bottom quark Dirac field. We define the n'th moment P_n of the vacuum polarization function as

$$P_n \;\equiv\; \frac{4\,\pi^2\,Q_b^2}{n!\,q^2} \left(\frac{d}{dq^2}\right)^n \Pi_\mu{}^\mu(q)\Big|_{q^2=0}\,, \tag{3}$$

where $Q_b = -1/3$ is the electric charge of the bottom quark. Due to causality the n-th moment P_n can be written in terms of a dispersion integration

$$P_n \;=\; \int \frac{ds}{s^{n+1}}\, R(s)\,, \tag{4}$$

where

$$R(s) \;=\; \frac{\sigma(e^+e^- \to \gamma^* \to \text{“}b\bar{b}\text{”})}{\sigma_{pt}} \tag{5}$$

is the total photon mediated cross section of bottom quark-antiquark production in e^+e^- annihilation normalized to the point cross section $\sigma_{pt} = 4\pi\alpha^2/3s$. Assuming global duality, P_n can be either calculated from experimental data for the total cross section in e^+e^- annihilation[2] or theoretically

[2] At the level of precision in this work the Z mediated cross section can be safely neglected.

using quantum chromodynamics (QCD). It is the basic idea of this sum rule to set the moments calculated from experimental data, P_n^{ex}, equal to those determined theoretically from QCD, P_n^{th}, and to use this relation to determine the bottom quark mass (and the strong coupling) by fitting theoretical and experimental moments for various values of n. [5, 6, 13]

At this point it is mandatory to discuss the range of n for which the theoretical moments can be calculated sufficiently accurate (using perturbative QCD) to allow for a reliable extraction of M_b and α_s. From Eq. (4) is obvious that each moment P_n effectively corresponds to a *smearing* of the cross section R over some energy region ΔE located around the threshold point. Thus, only if the smearing range is *sufficiently* larger than $\Lambda_{\rm QCD} \sim \mathcal{O}(200 - 300 \text{ MeV})$, a perturbative calculation of the moments is feasible [14]. [In Ref. [14] is was argued that ΔE should be larger than $4M_b\alpha_s$ to avoid the complications involving a resummation of the Coulomb singularities $\propto (\alpha_s/v)^m$. Because this resummation is explicitly carried out at the NNLO level in this work, we have to take $\Lambda_{\rm QCD}$, the typical hadronic scale, as the size of the minimal smearing range.] We therefore conclude that n is not allowed to be too large if perturbative QCD shall be employed. We can derive an approximate upper bound for the allowed values of n by changing the integration variable in relation (4) to the energy $E \equiv \sqrt{q^2} - 2M_b$. For $n \gg 1$ only energies $E \ll M_b$ contribute, which allows us to expand expression (4) for small E/M_b (while regarding $(E/M_b)n$ of order one)

$$P_n \overset{n\gg 1}{=} \frac{1}{(4\,M_b^2)^n} \int \frac{dE}{M_b} \exp\Big(-\frac{E}{M_b}\,n\Big)\, R\Big((2\,M_b + E)^2\Big) \left[1 + \mathcal{O}\Big(\frac{E}{M_b}, \frac{E^2}{M_b^2}\,n\Big)\right]. \tag{6}$$

From Eq. (6) we see that the size of the smearing range ΔE for large n is or order M_b/n,

$$\Delta E \sim \frac{M_b}{n}\,. \tag{7}$$

Demanding that ΔE is larger than $\Lambda_{\rm QCD}$ yields that the values of n for which a perturbative calculation of the moments can trusted should be sufficiently smaller than $15-20$. To avoid systematic theoretical errors as much as possible we take

$$n_{max} = 10 \tag{8}$$

as the maximal value for n employed in this work. On the other hand, it is also desirable to choose n as large as possible because the experimental cross section for electron positron annihilation into $b\bar{b}$ hadrons is much better known in the Υ resonance regime $\sqrt{s} \sim 9.5 - 10.5$ GeV than above the $B\bar{B}$ threshold. By taking n large the lower lying resonance contributions in Eq. (4) are enhanced relative to the continuum contributions leading effectively to a suppression of the experimental uncertainties in the continuum cross section [5, 6, 15]. For our analysis we choose

$$n_{min} = 4 \tag{9}$$

as the minimal value for n. It is the regime $4 \leq n \leq 10$ which we will refer to as "large n" in this work. It is a very important fact that for $4 \leq n \leq 10$ the bottom-antibottom quark dynamics in the theoretical moments P_n^{th} is already nonrelativistic in nature. This can be seen by once again examining relation (6). Because for a given value of n only energies $E \lesssim M_b/n$ contribute, the corresponding bottom quark velocities $v = \sqrt{E/M_b}$ (in the c.m. frame) are in the range $|v| \lesssim 0.5$, i.e. they are always considerably smaller than the speed of light. In particular, the velocity is already as large as the typical size of the strong coupling $\alpha_s(M_b v) \approx 0.3$ governing the exchange of longitudinal polarized

gluons (in Coulomb gauge) among the bottom-antibottom quark pair. This leads to the breakdown of the conventional multi-loop perturbation expansion because the exchange of m longitudinal gluons generates singular terms $\propto (\alpha_s/v)^m$, $m = 0, 1, 2, \ldots$, (Coulomb singularities) in the cross section for small velocities. These singular terms would have to be resummed[3] to all orders in multi-loop perturbation theory in order to arrive at a viable description of the bottom-antibottom quark dynamics. In other words, the Coulomb interaction between the bottom and the antibottom quark has to be treated exactly [6]. Because this is an impossible talk in the framework of covariant multi-loop perturbation theory it is mandatory to calculate the cross section and the theoretical moments in the nonrelativistic approximation by solving the Schrödinger equation supplemented by relativistic corrections.

Perturbative NRQCD and the Cross Section

In this paper we use NRQCD [11, 12] to set up a consistent framework in which the corrections to the nonrelativistic limit (in form of the nonrelativistic Schrödinger equation) can be determined in a systematic manner at NNLO. This corresponds to corrections up to order α_s^2, $\alpha_s\, v$ and v^2 to the expressions in the nonrelativistic limit. We count orders of α_s as orders of v because we treat the $b\bar{b}$ system as Coulombic. In the framework of multi-loop perturbation theory this would correspond to a resummation of all terms $\propto \alpha_s^m v^k$ with $m + k = 1, 2, 3$ in the cross section for the small velocity expansion. NRQCD is an effective field theory of QCD designed to handle nonrelativistic heavy-quark-antiquark systems to in principle arbitrary precision. NRQCD is based on the separation of long- and short-distance effects by reformulating QCD in terms of an unrenormalizable Lagrangian containing all possible operators in accordance to the symmetries in the nonrelativistic limit. Treating all quarks of the first and second generation as massless and taking into account only those terms relevant for the NNLO calculation in this work the NRQCD Lagrangian reads [12]

$$\begin{aligned}
\mathcal{L}_{\rm NRQCD} \;=\; & -\frac{1}{2}\,{\rm Tr}\, G^{\mu\nu} G_{\mu\nu} + \sum_{q=u,d,s,c} \bar{q}\, i\not{D}\, q \\
& + \psi^\dagger \left[i D_t + a_1\, \frac{\boldsymbol{D}^2}{2\, M_t} + a_2\, \frac{\boldsymbol{D}^4}{8\, M_t^3} \right] \psi + \ldots \\
& + \psi^\dagger \left[\frac{a_3\, g}{2\, M_t}\, \boldsymbol{\sigma}\cdot\boldsymbol{B} + \frac{a_4\, g}{8\, M_t^2}\, (\, \boldsymbol{D}\cdot\boldsymbol{E} - \boldsymbol{E}\cdot\boldsymbol{D}\,) + \frac{a_5\, g}{8\, M_t^2}\, i\, \boldsymbol{\sigma}\, (\, \boldsymbol{D}\times\boldsymbol{E} - \boldsymbol{E}\times\boldsymbol{D}\,) \right] \psi + \ldots \\
& + \chi\chi^\dagger \text{ bilinear terms and higher dimensional operators}\,. \qquad (10)
\end{aligned}$$

The gluons and massless quarks are described by the conventional relativistic Lagrangian, where $G_{\mu\nu}$ is the gluon field strength tensor, q the Dirac spinor of a massless quark and D_μ the gauge covariant derivative. For convenience, all color indices in Eq. (10) and throughout this work are suppressed. The nonrelativistic bottom and antibottom quarks are described by the Pauli spinors ψ and χ, respectively. D_t and $\boldsymbol{D}$ are the time and space components of the gauge covariant derivative D and $E^i = G^{0i}$ and $B^i = \frac{1}{2}\epsilon^{ijk} G^{jk}$ the electric and magnetic components of the gluon field strength tensor (in Coulomb gauge). The straightforward $\chi^\dagger\chi$ bilinear terms are omitted and can be obtained using charge symmetry. The short-distance coefficients $a_1, \ldots, a_5$ are normalized to one at the Born

[3] In this context "resummation" technically means that one carries out the resummation of singular terms in the (formal) kinematic regime $\alpha_s \ll |v|$. The resulting series (uniquely) define analytic functions which can then be continued to the regime $|v| \lesssim \alpha_s$.

level. The actual form of the higher order contributions to the short-distance coefficients $a_1, \ldots, a_5$ (and also to b_1, b_2 in Eq. (12)) is irrelevant for this work, because we will later use the "direct matching" procedure [7, 16] at the level of the final result for the cross section.

Let us first discuss the cross section R in the nonrelativistic regime. To formulate R in the nonrelativistic regime at NNLO in NRQCD we start from the fully covariant expression for the total cross section

$$\begin{aligned} R(q^2) &= \frac{4\,\pi\,Q_b^2}{q^2}\,\mathrm{Im}\,[\,-i\int dx\,e^{i\,q.x}\,\langle\,0\,|T\,j_\mu^b(x)\,j^{b\,\mu}(0)\,|\,0\,\rangle] \\ &\equiv \frac{4\,\pi\,Q_b^2}{q^2}\,\mathrm{Im}\,[\,\langle\,0\,|T\,\tilde{j}_\mu^b(q)\,\tilde{j}^{b\,\mu}(-q)\,|\,0\,\rangle]\,, \end{aligned} \tag{11}$$

and expand the electromagnetic current (in momentum space) $\tilde{j}_\mu(\pm q) = (\tilde{\bar{b}}\gamma^\mu\tilde{b})(\pm q)$ which produces/annihilates a $b\bar{b}$ pair with c.m. energy $\sqrt{q^2}$ in terms of ${}^3S_1$ NRQCD currents up to dimension eight ($i = 1, 2, 3$)

$$\begin{aligned} \tilde{j}_i(q) &= b_1\left(\tilde{\psi}^\dagger\sigma_i\tilde{\chi}\right)(q) - \frac{b_2}{6M_t^2}\left(\tilde{\psi}^\dagger\sigma_i(-\tfrac{i}{2}\overleftrightarrow{\boldsymbol{D}})^2\tilde{\chi}\right)(q) + \ldots\,, \\ \tilde{j}_i(-q) &= b_1\left(\tilde{\chi}^\dagger\sigma_i\tilde{\psi}\right)(-q) - \frac{b_2}{6M_t^2}\left(\tilde{\chi}^\dagger\sigma_i(-\tfrac{i}{2}\overleftrightarrow{\boldsymbol{D}})^2\tilde{\psi}\right)(-q) + \ldots\,, \end{aligned} \tag{12}$$

where the constants b_1 and b_2 are short-distance coefficients normalized to one at the Born level. Only the spatial components of the currents contribute contribute at the NNLO level. Inserting expansion (12) back into Eq. (11) leads to the nonrelativistic expansion of the cross section at the NNLO level

$$\begin{aligned} R^{\rm thr}_{\rm NNLO}(\tilde{E}) &= \frac{\pi\,Q_b^2}{M_b^2}\,C_1(\mu_{\rm hard},\mu_{\rm fac})\,\mathrm{Im}\Big[\,\mathcal{A}_1(E,\mu_{\rm soft},\mu_{\rm fac})\,\Big] \\ &\quad - \frac{4\,\pi\,Q_b^2}{3M_b^4}\,C_2(\mu_{\rm hard},\mu_{\rm fac})\,\mathrm{Im}\Big[\,\mathcal{A}_2(E,\mu_{\rm soft},\mu_{\rm fac})\,\Big] + \ldots\,, \end{aligned} \tag{13}$$

where

$$\mathcal{A}_1 = \langle\,0\,|\,(\tilde{\psi}^\dagger\vec{\sigma}\,\tilde{\chi})\;(\tilde{\chi}^\dagger\vec{\sigma}\,\tilde{\psi})\,|\,0\,\rangle\,, \tag{14}$$

$$\mathcal{A}_2 = \tfrac{1}{2}\,\langle\,0\,|\,(\tilde{\psi}^\dagger\vec{\sigma}\,\tilde{\chi})\;(\tilde{\chi}^\dagger\vec{\sigma}\,(-\tfrac{i}{2}\overleftrightarrow{\boldsymbol{D}})^2\tilde{\psi}) + \text{h.c.}\,|\,0\,\rangle\,. \tag{15}$$

The cross section is expanded in terms of a sum of absorptive parts of nonrelativistic current correlators, each of them multiplied by a short-distance coefficient. In fact, the right-hand side (RHS) of Eq. (13) just represents an application of the factorization formalism proposed in [12]. The second term on the RHS of Eq. (13) is suppressed by v^2, i.e. of NNLO. This can be seen explicitly by using the equations of motion from from the NRQCD Lagrangian, which relates the correlator $\mathcal{A}_2$ directly to $\mathcal{A}_1$,

$$\mathcal{A}_2 = M_b\,E\,\mathcal{A}_2\,. \tag{16}$$

Relation (16) has also been used to obtain the coefficient $-4/3$ in front of the second term on the RHS of Eq. (13). The nonrelativistic current correlators $\mathcal{A}_1$ and $\mathcal{A}_2$ contain the resummation of the

singular terms mentioned in the previous paragraph. They incorporate all the long-distance[4] dynamics governed by soft scales like the relative three momentum $\sim M_b\alpha_s$ or the binding energy of the $b\bar{b}$ system $\sim M_b\alpha_s^2$.[5] The constants C_1 and C_2 (which are also normalized to one at the Born level), on the other hand, describe short-distance effects involving hard scales of the order of the bottom quark mass. They only represent a simple power series in α_s and do not contain any resummations in α_s. Because we consider the total $b\bar{b}$ cross section normalized to the point cross section, Eq. (5), C_1 and C_2 are independent of q^2. In Eq. (13) we have also indicated the dependence of the correlators and the short-distance coefficients on the various renormalization scales: The factorization scale $\mu_{\rm fac}$ essentially represents the boundary between hard and soft momenta. The dependence on the factorization scale becomes explicit because of ultraviolet (UV) divergences contained in NRQCD. Because, as in any effective field theory, this boundary is not defined unambiguously, both the correlators and the short-distance coefficients in general depend on $\mu_{\rm fac}$. The soft scale $\mu_{\rm soft}$ and the hard scale $\mu_{\rm hard}$, on the other hand, are inherent to the correlators and the short-distance constants, respectively, governing their perturbative expansion. If we would have all orders in α_s and v at hand, the dependence of the cross section $R^{\rm thr}_{\rm NNLO}$ on variations of each the three scales would vanish exactly. (It is important that the soft and the hard scale, which both originate from the light degrees of freedom in the NRQCD Lagrangian, and the factorization scale are each considered as independent. They can each be defined in different regularization schemes. In this work we will use the $\overline{\rm MS}$ scheme for the soft and the hard scale and a cutoff scheme for the factorization scale.) Unfortunately, we only perform the calculation up to NNLO in α_s and v which leads to a residual dependence on the three scales $\mu_{\rm fac}$, $\mu_{\rm soft}$ and $\mu_{\rm hard}$. In particular, (as we will demonstrate in Section 4) the dependence on the soft scale $\mu_{\rm soft}$ is quite strong, clearly because it governs the perturbative expansion of the correlators where convergence of the perturbation series can be expected to be worse than for the short-distance constants. It is therefore necessary to fix a certain window for each of the renormalization scales for which the perturbative series for the cross section shall be evaluated. At this point one can basically only rely on physical intuition, which tells that the renormalization scales should be of the same order as the physical scales governing the particular problem. This means that the soft scale should be the order of the relative momentum of the $b\bar{b}$ system[6] $\sim M_b\,\alpha_s$, and that the hard scale should be of order $M_b \sim 5$ GeV. The factorization scale, on the other hand, should cover (at least partly) the soft and and hard regime. Because there is in our opinion no unique way to make this statement more quantitative, it is important to choose the corresponding windows "reasonably large". In our case the choices are as follows:

$$\begin{aligned} 1.5\,\text{GeV} \;\leq\; & \mu_{\rm soft} \;\leq\; 3.5\,\text{GeV}\,, \\ 2.5\,\text{GeV} \;\leq\; & \mu_{\rm hard} \;\leq\; 10\,\text{GeV}\,, \\ 2.5\,\text{GeV} \;\leq\; & \mu_{\rm fac} \;\leq\; 10\,\text{GeV}\,. \end{aligned} \tag{17}$$

We will show in Sections 5 and 6 that the dependence of the theoretical moments P_n^{th} on theses scales represents the dominant source of the uncertainties in the extraction of M_b. Thus, it is the choice

[4] In the context of this paper "long-distance" is not equivalent to "nonperturbative".

[5] It is not clear at all whether there a not even smaller energy scales $\sim M_b\,\alpha_s^k$, $k > 2$, which might become relevant. However, those scales can only be produced by higher order effects like the hyperfine splitting, which should be irrelevant at least for the total cross section at NNLO.

[6] We will see later that at NNLO all interactions can be treated as instantaneous. As a consequence scales of the order of the binding energy $\sim M_b\,\alpha_s^2$ can be ignored.

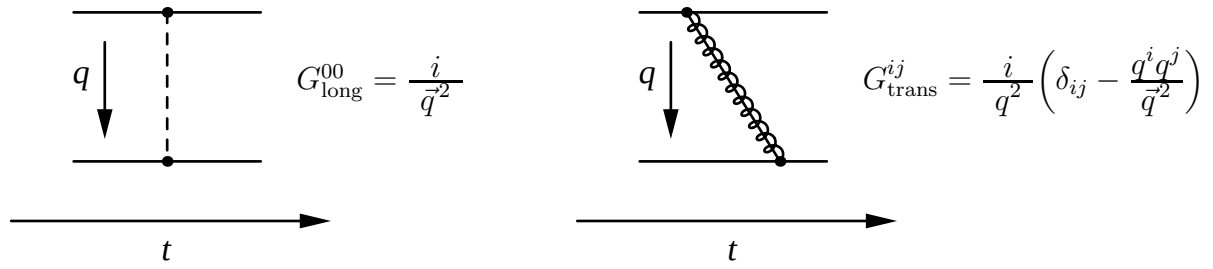

Figure 1: Graphical representation of the longitudinal and the transverse gluon exchange including the corresponding Feynman rules for the momentum exchange $q = (q^0, \vec{q})$. The exchange of a longitudinal gluon is instantaneous in time because its does not have an energy dependence. As a consequence the longitudinal exchange can be described by an instantaneous potential. The exchange of a transverse gluon, on the other hand, is retarded in time and, in general, cannot be described in terms of an instantaneous potential.

given in Eqs. (17) which determines the size of the uncertainties!

Instantaneous Interactions and Retardation Effects

To calculate the correlators $\mathcal{A}_1$ and $\mathcal{A}_2$ we use methods originally developed for QED bound state calculations in the framework of NRQED [7, 11, 17, 18] and transfer them (with the appropriate modifications to account for the non-Abelian effects) to the problem of heavy quark-antiquark production in the kinematic regime close to the threshold. Because the Coulomb gauge is the standard gauge in which QED bound state calculations are carried out we also use the Coulomb gauge for the calculations in this work. The Coulomb gauge separates the gluon propagator into a longitudinal and a transverse piece (see Fig. 1). The longitudinal propagator does not have an energy dependence and therefore represents an instantaneous interaction. As a consequence, in configuration space representation a longitudinal gluon exchange can be written as an instantaneous potential (which only depends on the spatial distance). Through the time derivative in the NRQCD Lagrangian the longitudinal gluon exchange leads to the Coulomb potential which is the dominant (LO) interaction between the bottom quarks in the nonrelativistic limit. Through the $1/M_b^2$ couplings of the bottom quarks to the chromo-electric field the longitudinal exchange also leads to the Darwin and spin-orbit potential, which contribute at the NNLO level. Because these potentials are instantaneous their treatment is straightforward in the framework of a two-body Schrödinger equation.

For the transverse gluon the situation is more subtle. Because all couplings of the bottom quarks to the chromo-magnetic field are of order $1/M_b$ the exchange of a transverse gluon between two bottom quark lines is a NNLO effect. However, in contrast to the Darwin and the spin-orbit interaction, the propagation of the transverse gluon energy has an energy dependence, i.e. it is an interaction with a temporal retardation. Physically this means that the transverse gluon can travel alongside the $b\bar{b}$ pair for some time period [6, 19]. In this time period the $b\bar{b}$ pair is part of a higher order Fock $b\bar{b}$-gluon state which, in principle, cannot be treated in terms of a two-body Schrödinger equation. Fortunately, in our case we can neglect the energy dependence of the transverse gluon

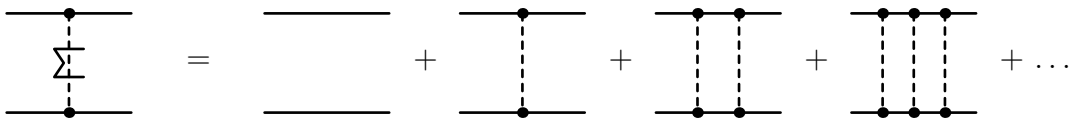

Figure 2: Graphical representation of the resummation of Coulomb ladder diagrams to all orders. The quark-antiquark propagation contains the nonrelativistic kinetic energy. The resummation is carried out explicitly by calculating the Green function the nonrelativistic Schrödinger equation with the Coulomb potential at the Born level, see Eq. (27).

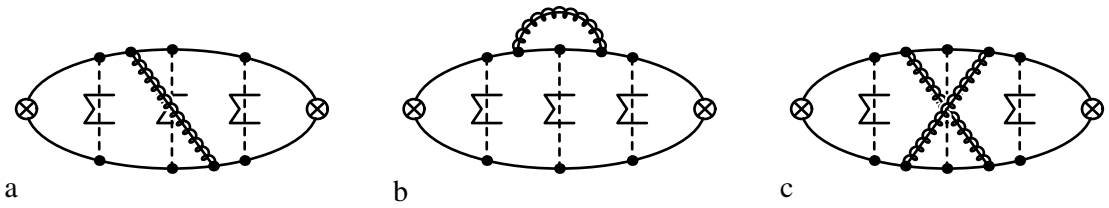

Figure 3: Typical diagrams describing the exchange of a transverse gluons (in Coulomb gauge) in the background of the Coulomb exchange of longitudinal gluons. Longitudinal lines with a $\sum$ sign represent the summation of Coulomb ladder diagrams to all orders, see Fig. 2.

propagator completely. This can be easily understood by considering a typical diagram describing the exchange of a transverse gluon between the $b\bar{b}$ pair in the background of a continuous Coulomb exchange of longitudinal gluons, see e.g. Fig. 3a. If both ends of the transverse gluon end at bottom quarks the typical energy carried by the gluon can only be of order $M_b\, v^2$, the c.m. kinetic energy of the bottom quarks. The typical three momentum of the gluon, on the other hand, can either be of order $M_b\, v$, the relative momentum in the $b\bar{b}$ system, or also of order $M_b\, v^2$. If the three momentum is of order $M_b\, v^2$, the transverse gluon is essentially real and needs, in addition to the v^2 suppression coming from the couplings to the quarks, another phase space factor v to exist. Thus, the transverse gluons with this energy-momentum configuration lead to effects suppressed by v^3, which is beyond the NNLO level. If the three momentum of the transverse gluon is of order $M_b\, v$, on the other hand, it is far off-shell and we can neglect the small energy component in a first approximation. [It should be emphasized that this argument implies the hierarchy $M_b\alpha_s \gg M_b\alpha_s^2$, which is conceivable for the $b\bar{b}$ system where $\alpha_s \sim 0.3$.] From that one can see that at NNLO the transverse gluon exchange can, like the longitudinal one, also be treated as an instantaneous interaction. This means that in Fig. 3a only those diagrams contribute at NNLO where the transverse line does not cross any longitudinal line. The differences between longitudinal and transverse gluons will only become manifest beyond the NNLO level. For the same reason any self-energy or crossed-ladder type diagram (see Figs. 3b,c for typical examples) can be safely neglected at the NNLO level. In fact, the situation is in complete analogy to the hydrogen atom or the positronium in QED, where it is well known that retardation effects lead to the "Lamb-shift" corrections which are suppressed by α^3 relative to the LO nonrelativistic

contributions. [Of course, the crossed exchange and self-energy type diagrams have to be taken into account in the two-loop calculation of the cross section in full QCD needed to determine the $\mathcal{O}(\alpha_s^2)$ contributions to the short-distance coefficients. Those short-distance constants, however, describe effect from high momenta of order M_b which are not contained in the correlators.]

From the considerations above we can draw the following conclusions regarding the calculation of the correlators $\mathcal{A}_1$ and $\mathcal{A}_2$ at NNLO:

1. We can treat the problem of $b\bar{b}$ production close to threshold as a pure two-body problem. This means that the NRQCD Lagrangian effectively reduces to a two-body Schrödinger equation from which the correlators can be determined.

2. All interactions between the bottom and the antibottom quark can be written as time independent, instantaneous potentials, which means that only ladder-like diagrams have to taken into account.

3. We can use the well known analytic solutions of the nonrelativistic Coulomb problem for positronium [20, 21, 22] and use Rayleigh-Schrödinger time-independent perturbation theory (TIPT) to determine the corrections caused by all higher order interactions and effects.

However, there is one remark in order: although the effects of the transverse gluon exchange having a temporal retardation are formally beyond the NNLO level, this is not a proof that they are indeed smaller than the NNLO contributions calculated in this work. It is in fact rather likely that the retardation effects cannot be calculated at all using perturbative methods because the characteristic scale of the coupling governing the emission, absorption or interaction of a gluon which has energy and momentum of order $M_b\alpha_s^2$ would be of the order of $0.5-1$ GeV. This is already quite close to the typical hadronization scale $\Lambda_{\rm QCD}$. From this point of view it seems that the NNLO analysis presented here cannot be improved any more, at least not with perturbative methods. This problem might even cast doubts on the reliability of the NNLO corrections themselves and underlines the necessity that the preferred ranges for the renormalization scales, Eqs. (17), are chosen sufficiently large. We will ignore further implications of this problem for the calculations and analyses carried out in this work. (See also the paragraph on nonperturbative effects.)

Instantaneous Potentials

At the Born level all potentials relevant for the nonrelativistic cross section at NNLO can be obtained directly from the NRQCD Lagrangian considering (color singlet) $b\bar{b} \to b\bar{b}$ single gluon t-channel exchange scattering diagrams. In configuration space representation the Born level potentials read ($r \equiv |\vec{r}|$, $C_F = 4/3$, $C_A = 3$, $T = 1/2$, $a_s \equiv \alpha_s(\mu_{\rm soft})$)

$$
\begin{aligned}
V_c^{(0)}(\vec{r}) &= -\frac{C_F\, a_s}{r}\,, \\
V_{\rm BF}(\vec{r}) &= \frac{C_F\, a_s\, \pi}{M_b^2}\left[1+\frac{8}{3}\,\vec{S}_b\,\vec{S}_{\bar{b}}\right]\delta^{(3)}(\vec{r}) + \frac{C_F\, a_s}{2M_b^2 r}\left[\vec{\nabla}^2 + \frac{1}{r^2}\vec{r}\,(\vec{r}\,\vec{\nabla})\vec{\nabla}\right] \\
&\quad - \frac{3\,C_F\, a_s}{M_b^2 r^3}\left[\frac{1}{3}\,\vec{S}_b\,\vec{S}_{\bar{b}} - \frac{1}{r^2}\left(\vec{S}_b\,\vec{r}\right)\left(\vec{S}_{\bar{b}}\,\vec{r}\right)\right] + \frac{3\,C_F\, a_s}{2M_b^2 r^3}\,\vec{L}\,(\vec{S}_b + \vec{S}_{\bar{b}})\,,
\end{aligned}
\tag{18}
$$

where $\vec{S}_b$ and $\vec{S}_{\bar{b}}$ are the bottom and antibottom quark spin operators and $\vec{L}$ is the angular momentum operator. $V_c^{(0)}$ is the well known Coulomb potential. It constitutes the LO interaction and will

(together with the nonrelativistic kinetic energy) be taken into account exactly. It arises from the exchange of a longitudinal gluon through the time derivative coupling of the bottom quarks to the gluon field. $V_{\rm BF}$ represents the Breit-Fermi potential which is known from higher order positronium calculations. It describes the Darwin and spin-orbit interactions which are mediated by the longitudinal gluons and also the so called hyperfine or tensor interactions which are mediated by the transverse gluons in the instantaneous approximation. Due to the $1/M_b^2$ suppression $V_{\rm BF}$ already leads to NNLO effects in the cross section and will be taken into account as a perturbation. For the same reason only the radiative corrections to the Coulomb exchange of longitudinal gluons have to be taken into account. We want to emphasize that these radiative corrections are caused by the massless degrees of freedom in the NRQCD Lagrangian. Because in the corresponding loops transverse gluon lines can end at other massless lines the considerations given in the preceding paragraph cannot be applied in this case. Thus, in general, transverse gluons (or massless quarks) in all energy-momentum configurations have to taken into account to calculate the radiative corrections properly. The calculation of these radiative corrections can be found in existing literature and we therefore just present the results.

At the one-loop level (and using the $\overline{\rm MS}$ scheme for the strong coupling) the corrections read ($\gamma_{\rm E} = 0.57721566\ldots$ being the Euler-Mascheroni constant)

$$V_c^{(1)}(\vec{r}) \;=\; V_c^{(0)}(\vec{r}) \left(\frac{a_s}{4\,\pi}\right) \left[\, 2\,\beta_0\, \ln(\tilde{\mu}\, r) + a_1 \,\right], \qquad \tilde{\mu} \;\equiv\; e^{\gamma_{\rm E}}\, \mu_{\rm soft}\,, \tag{19}$$

where

$$\begin{aligned} \beta_0 &= \frac{11}{3}\, C_A - \frac{4}{3}\, T\, n_l\,, \\ a_1 &= \frac{31}{9}\, C_A - \frac{20}{9}\, T\, n_l\,, \\ n_l &= 4\,, \end{aligned} \tag{20}$$

and

$$V_{\rm NA}(\vec{r}) \;=\; -\,\frac{C_A\, C_F\, a_s^2}{2\, M_b\, r^2}\,. \tag{21}$$

$V_c^{(1)}$ represents the one-loop corrections to the Coulomb potential $\propto 1/r$ and leads to NLO contributions in the cross section. $V_c^{(1)}$ has been calculated by Fischler [23] and Billoire [24]. $V_{\rm NA}$, called non-Abelian potential for the rest of this work, arises from a non-analytic behavior of the vertex diagram depicted in Fig. 4 $\propto (\vec{k}^2/M_b^2)^{1/2}$ where $\vec{k}$ is the three momentum exchanged between the bottom and the antibottom quark. Because the non-analytic term causes a behavior $\propto 1/|\vec{k}|$ for the non-Abelian potential in momentum space representation, $V_{\rm NA}$ is proportional to $1/r^2$. We would like to point out that in Coulomb gauge such a non-analytic behavior does not exist for Abelian diagrams. We refer the reader to [25] for older publications, where the non-Abelian potential has been determined. Due to the a_s/M_b factor $V_{\rm NA}$ is a NNLO interaction and no further corrections to it have to taken into account.

At the two-loop level only the corrections to the Coulomb potential have to be considered. They have been calculated recently by Peter [26] and read (in the $\overline{\rm MS}$ scheme)

$$V_c^{(2)}(\vec{r}) \;=\; V_c^{(0)}(\vec{r}) \left(\frac{a_s}{4\,\pi}\right)^2 \left[\, \beta_0^2 \left(\, 4\, \ln^2(\tilde{\mu}\, r) + \frac{\pi^2}{3} \,\right) + 2 \left(2\,\beta_0\, a_1 + \beta_1\right) \ln(\tilde{\mu}\, r) + a_2 \,\right], \tag{22}$$

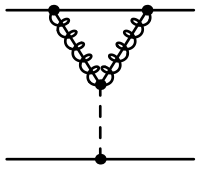

Figure 4: Vertex diagram in Coulomb gauge responsible for the potential non-Abelian potential $V_{\rm NA}$.

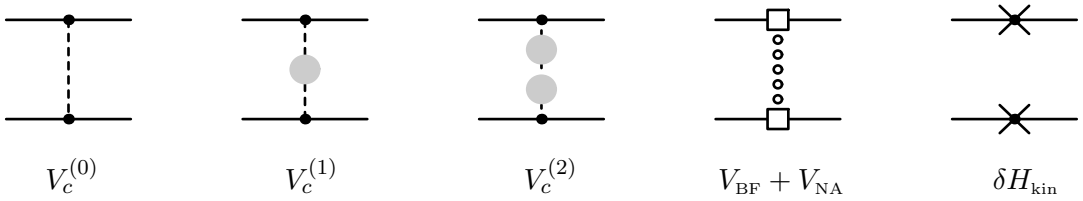

Figure 5: Symbols describing the interactions potentials $V_c^{(0)}$, $V_c^{(1)}$, $V_c^{(2)}$, $V_{\rm BF}$ and $V_{\rm NA}$ and the kinetic energy correction $\delta H_{\rm kin} = -\vec{\nabla}^4/4M_b^3$.

where

$$\begin{aligned}
\beta_1 &= \frac{34}{3}\,C_A^2 - \frac{20}{3} C_A\,T\,n_l - 4\,C_F\,T\,n_l\,, \\
a_2 &= \left(\frac{4343}{162} + 6\,\pi^2 - \frac{\pi^4}{4} + \frac{22}{3}\,\zeta_3\right) C_A^2 - \left(\frac{1798}{81} + \frac{56}{3}\,\zeta_3\right) C_A\,T\,n_l \\
&\quad - \left(\frac{55}{3} - 16\,\zeta_3\right) C_F\,T\,n_l + \left(\frac{20}{9}\,T\,n_l\right)^2 .
\end{aligned} \tag{23}$$

For later reference we assign the symbols in Fig. 5 to the potentials given above. We also would like to note that we do not have to consider any annihilation effects. The leading annihilation diagram is depicted in Fig 6. Because the annihilation process takes place at short distances, it produces local four-fermion operators in the NRQCD Lagrangian, which can be written as instantaneous potentials. The dominant annihilation potential which comes from the three gluon annihilation diagram has the form $V_{\rm ann}(\vec{r}) \propto (a_s^3/M_b^2)\delta^{(3)}(\vec{r})$ and would lead to effects suppressed by v^4 in the cross section.

Recipe for the Calculation of Large n Moments at NNLO

Based on the issues discussed above the calculation of the NNLO nonrelativistic cross section $R_{\rm NNLO}^{\rm thr}$ and the theoretical moments P_n^{th} in terms of the correlators $\mathcal{A}_1$ and $\mathcal{A}_2$ and the short-distance coefficients $C_{1/2}$ proceeds in the following three basic steps:

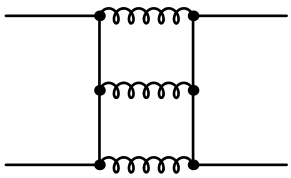

Figure 6: The dominant annihilation diagram relevant for $b\bar{b} \to b\bar{b}$ scattering for a bottom-antibottom quark pair in a color singlet $J^{PC} = 1^{--}$, ${}^3S_1$ configuration. Its dominant contribution leads to a potential $V_{\rm ann}(\vec{r}) \propto a_s^3/M_b^2\,\delta(\vec{r})$ and to contributions in the cross section and the moments beyond the NNLO level.

Step 1: *Solution of the Schrödinger equation.* – The Green function of the NNLO Schrödinger equation is calculated incorporating the potentials displayed above and including the NNLO corrections to the kinetic energy. The correlators $\mathcal{A}_1$ and $\mathcal{A}_2$ are directly related to the zero-distance Green function of the Schrödinger equation.

Step 2: *Matching calculation.* – The short-distance constant C_1 is determined at $\mathcal{O}(\alpha_s^2)$ by matching expression (13) directly to the cross section calculated in full QCD at the two-loop level and including terms up to NNLO in an expansion in v in the (formal) limit $\alpha_s \ll v \ll 1$.

Step 3: *Dispersion Integration.* – The integration (4) is carried out.

For the rest of this section we briefly explain the strategies and basic procedures for the steps 1 and 2. The explicit calculations for steps 1 – 3 are presented in detail in Sections 3.1, 3.2 and 3.3, respectively.

Solution of the Schrödinger equation: The nonrelativistic correlators $\mathcal{A}_1$ and $\mathcal{A}_2$ are calculated by determining the Green function of the Schrödinger equation ($E \equiv \sqrt{q^2} - 2M_b$)

$$\left(-\frac{\vec{\nabla}^2}{M_b} - \frac{\vec{\nabla}^4}{4\,M_b^3} + \left[V_c^{(0)}(\vec{r}) + V_c^{(1)}(\vec{r}) + V_c^{(2)}(\vec{r}) + V_{\rm BF}(\vec{r}) + V_{\rm NA}(\vec{r}) \right] - E \right) G(\vec{r},\vec{r}',E) = \delta^{(3)}(\vec{r}-\vec{r}')\,, \tag{24}$$

where V_{BF} is evaluated for the ${}^3S_1$ configuration only. The relation between the correlator $\mathcal{A}_1$ and Green function reads

$$\mathcal{A}_1 \;=\; 6\,N_c \left[\lim_{|\vec{r}|,|\vec{r}'|\to 0} G(\vec{r},\vec{r}',E) \right]. \tag{25}$$

Eq. (25) can be quickly derived from the facts that $G(\vec{r},\vec{r}',\tilde{E})$ describes the propagation of a bottom-antibottom pair which is produced and annihilated at relative distances $|\vec{r}|$ and $|\vec{r}'|$, respectively, and that the bottom-antibottom quark pair is produced and annihilated through the electromagnetic current at zero distances. Therefore $\mathcal{A}_1$ must be proportional to $\lim_{|\vec{r}|,|\vec{r}'|\to 0} G(\vec{r},\vec{r}',E)$. The correct proportionality constant can then be determined by considering production of a free (i.e. $\alpha_s = 0$) bottom-antibottom pair in the nonrelativistic limit. (In this case the Born cross section in full QCD can be easily compared to the imaginary part of the Green function of the free nonrelativistic Schrödinger equation.) The correlator $\mathcal{A}_2$ is determined from $\mathcal{A}_1$ via relation (16). We would like to emphasize

that the zero-distance Green function on the RHS of Eqs. (25) contains UV divergences which have to regularized. In the actual calculations carried out in Section 3.1 we impose the explicit short-distance cutoff $\mu_{\rm fac}$. As mentioned before, this is the reason why the correlators and the short-distance constants depend explicitly on the (factorization) scale $\mu_{\rm fac}$. In this work we solve equation (24) perturbatively by starting from well known Green function $G_c^{(0)}$ of the nonrelativistic Coulomb problem [20, 21, 22]

$$\left(-\frac{\nabla^2}{M_b} - V_c^{(0)}(\vec{r}) - E \right) G_c(\vec{r},\vec{r}',E) \;=\; \delta^{(3)}(\vec{r}-\vec{r}') \tag{26}$$

and by incorporating all the higher order terms using TIPT.

Matching calculation: After the nonrelativistic correlators $\mathcal{A}_1$ and $\mathcal{A}_2$ are calculated the determination of C_1 is achieved by considering the (formal) limit $\alpha_s \ll v \ll 1$. In this limit fixed multi-loop perturbation theory (i.e. an expansion in α_s) as well as the nonrelativistic approximation (i.e. a subsequent expansion in v) are feasible. This means that multi-loop QCD (with an expansion in v *after* the loop integrations have been carried out) and multi-loop NRQCD must give the same results. In our case we use this fact to determine the constant C_1 up to terms of order α_s^2. For that we expand the NNLO NRQCD expression for the cross section (13) for small α_s up to terms of order α_s^2 and demand equality (i.e. match) to the total cross section obtained at the two-loop level in full QCD keeping terms up to NNLO in an expansion in v. Because NRQCD is an effective field theory of QCD (i.e. it has the same infrared behavior as full QCD) for the limit $v \ll 1$, C_1 contains only constant coefficients (modulo logarithms of the ratios $M_b/\mu_{\rm fac}$ and $M_b/\mu_{\rm hard}$). All the singular terms $\propto 1/v, \ln v$ are incorporated in the correlators $\mathcal{A}_1$ and $\mathcal{A}_2$

Comment on Nonperturbative Effects

To conclude this section we would like to mention that nowhere in this work nonperturbative effects in terms of phenomenological constants like the gluon condensate $\langle\, 0 \,|G_{\mu\nu}\, G^{\mu\nu}|\, 0 \,\rangle$ [15] are taken into account. In [2, 6] it has been shown that the contribution of the most important condensate $\langle\, 0 \,|G_{\mu\nu}\, G^{\mu\nu}|\, 0 \,\rangle$ is at the per-mill level in the moments P_n^{th} for $4 \le n \le 10$. As we show in Section 4, this effect is completely negligible compared to the theoretical uncertainties coming from the large renormalization scale dependences of the NNLO moments P_n^{th}. The condensates are therefore irrelevant from the purely practical point of view.

Nevertheless, we even think that the inclusion of the condensates for the moments at the NNLO level would be conceptually unjustified. For the gluon condensate this can be seen from the fact that it provides a phenomenological parameterization of the average long-wavelength vacuum fluctuations of the gluon field involving scales smaller than the relative three momentum of the $b\bar{b}$ system [19]. Thus, for the theoretical moments P_n^{th} $(4 \le n \le 10)$ (and also for heavy enough quarkonia in general) the condensates describe retardation-like effects [6]. As explained before, we neglect retardation effects because they formally contribute beyond the NNLO level. We conclude that taking into account the condensates would only be sensible in a complete NNNLO analysis. In this respect the condensate contributions might provide some estimates for the size of some NNNLO effects. However, if the small size of the condensate effects in the moments P_n^{th} is compared to the large perturbative uncertainties contained of the NNLO theoretical moments, it is seems rather doubtful whether the condensates represent the dominant contributions at the NNNLO level.

3 Calculation of the Moments

In this section the determination of the theoretical moments P_n^{th} is presented in detail. Because all conceptual issues have been discussed is Section 1 we concentrate only on the technical aspects. The task is split into three parts which are described in the following three subsections. In Section 3.1 the nonrelativistic correlators $\mathcal{A}_1$ and $\mathcal{A}_2$ are calculated and Section 3.2 describes the calculation of the short-distance constant C_1. In Section 3.3 the dispersion integration (4) is carried and the final formulae for the theoretical moments are presented.

3.1 Calculation of the Nonrelativistic Correlators

To calculate the nonrelativistic correlators $\mathcal{A}_1$ and $\mathcal{A}_2$ the Green function G of the Schrödinger equation (24) has to be determined. As explained before, we start with the Green function $G_c^{(0)}$ of the nonrelativistic Schrödinger equation (26), called "Coulomb Green function" from now on, and determine the effects all the higher order contributions through TIPT. The most general form of the Coulomb Green function reads ($r \equiv |\vec{r}|$, $r' \equiv |\vec{r}'|$)

$$G_c^{(0)}(\vec{r},\vec{r}',E) \;=\; -\,\frac{M_b}{4\,\pi\,\Gamma(1+i\,\rho)\,\Gamma(1-i\,\rho)}\,\int\limits_0^1 dt\int\limits_1^\infty ds\,\Big[\,s\,(1-t)\,\Big]^{i\,\rho}\,\Big[\,t\,(s-1)\,\Big]^{-i\,\rho}\,\times$$

$$\times\,\frac{\partial^2}{\partial t\,\partial s}\,\left[\,\frac{t\,s}{|\,s\,\vec{r}-t\,\vec{r}'\,|}\,\exp\left\{\,i\,p\,\Big(\,|\,\vec{r}'\,|\,(1-t)+|\,\vec{r}\,|\,(s-1)+|\,s\,\vec{r}-t\,\vec{r}'\,|\,\Big)\,\right\}\,\right],\quad r'\,<\,r\,, \tag{27}$$

where

$$p\;\equiv\;M_b\,v\;=\;\sqrt{M_b\,(E+i\,\epsilon)}\,,\qquad \rho\;\equiv\;\frac{C_F\,a_s}{2\,v} \tag{28}$$

and Γ is the gamma function. The case $r < r'$ is obtained by interchanging r and r'. $G_c^{(0)}(\vec{r},\vec{r}',E)$ represents the analytical expression for the sum of ladder diagrams depicted in Fig. 2. We refer the reader interested in the derivation of $G_c^{(0)}$ to the classical papers [20, 21, 22]. The analytic form of the Coulomb Green function shown in Eq. (27) has been taken from Ref. [20]. Fortunately we do not need the Coulomb Green function in its most general form but only its S-wave component

$$\begin{aligned} G_c^{(0),S}(r,r',E) \;&=\; \frac{1}{4\,\pi}\,\int d\Omega\,G_c^{(0)}(\vec{r},\vec{r}',E) \\ &=\; -\,\frac{2\,i\,M_b\,p}{4\,\pi\,\Gamma(1+i\,\rho)\,\Gamma(1-i\,\rho)}\,\int\limits_0^1 dt\int\limits_1^\infty ds\,\Big[\,s\,(1-t)\,\Big]^{i\,\rho}\,\Big[\,t\,(s-1)\,\Big]^{-i\,\rho}\,\times \\ &\qquad\times\,\exp\Big\{\,i\,p\,\Big[\,r'\,(1-2\,t)+r\,(2\,s-1)\,\Big]\,\Big\}\,,\qquad r'\,<\,r\,. \end{aligned} \tag{29}$$

The case $r < r'$ is again obtained by interchanging r and r'. For $r' = 0$ the form of the Coulomb Green function is particularly simple

$$\begin{aligned} G_c^{(0)}(0,r,E) \;&=\; G_c^{(0)}(0,\vec{r},E) \;=\; -\,i\,\frac{M_b\,p}{2\,\pi}\,e^{i\,p\,r}\,\int\limits_1^\infty dt\,e^{2\,i\,p\,r\,t}\,\left(\,\frac{1+t}{t}\,\right)^{i\,\rho} \\ &=\; -\,i\,\frac{M_b\,p}{2\,\pi}\,e^{i\,p\,r}\,\Gamma(1-i\,\rho)\,U(1-i\,\rho,2,-2\,i\,p\,r) \end{aligned}$$

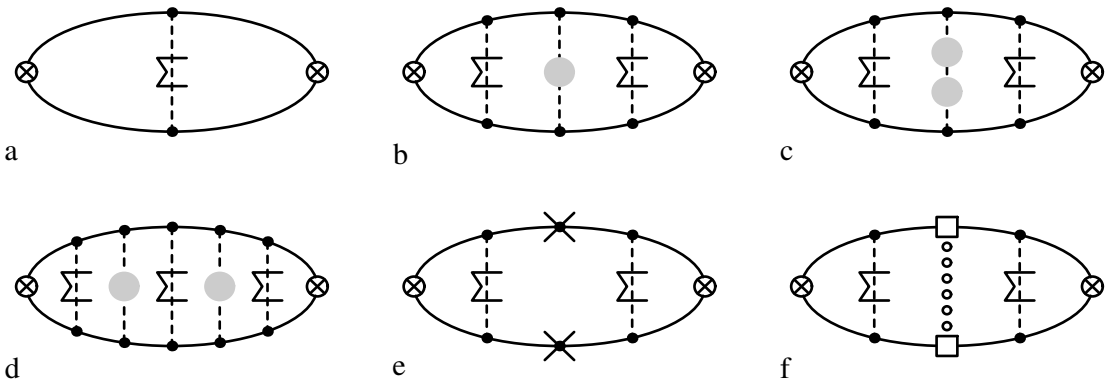

Figure 7: Graphical representation of the vacuum polarization ladder diagrams needed to determine the nonrelativistic cross section and the large n moments at NNLO.

$$= \frac{M_b}{4\,\pi\,r}\,\Gamma(1-i\,\rho)\,W_{i\,\rho,\frac{1}{2}}(-2\,i\,p\,r)\,. \tag{30}$$

where $U(a,b,z)$ is a confluent hypergeometric function and $W_{\kappa,\mu}(z)$ one of the Whittaker's functions [27, 28]. It is an important fact that $G_c^{(0)}(0,\vec{r},E)$ diverges for the limit $r\to 0$ because it contains power ($\propto 1/r$) and logarithmic ($\propto \ln r$) divergences [16]. As explained in Section 1 these ultraviolet (UV) divergences are regularized by imposing the small distance cutoff $\mu_{\rm fac}$. The regularized form of $\lim_{r\to 0} G_c(0,\vec{r},E)$ reads

$$G_c^{(0),\,reg}(0,0,E) \;=\; \frac{M_b^2}{4\,\pi}\left\{\,i\,v - C_F\,a_s\left[\,\ln(-i\frac{M_b\,v}{\mu_{\rm fac}}) + \gamma_{\rm E} + \Psi\Big(1 - i\,\frac{C_F\,a_s}{2v}\Big)\,\right]\right\}, \tag{31}$$

where the superscript "reg" indicates the cutoff regularization and $\Psi(z) = d\ln\Gamma(z)/dz$ is the digamma function. For the regularization we use the convention where all power divergences $\propto \mu_{\rm fac}$ are freely dropped and only logarithmic divergences $\propto \ln(\mu_{\rm fac}/M_b)$ are kept. Further, we define $\mu_{\rm fac}$ such that in the expression between the brackets all constants except the Euler-Mascheroni constant $\gamma_{\rm E}$ are absorbed. The same convention is also employed for the calculation of the higher order corrections to the Coulomb Green function which are discussed below. The results for any other regularization scheme which suppressed power divergences (like the $\overline{\rm MS}$ scheme) can be obtained by redefinition of the factorization scale. Our apparently sloppy realization of the regularization procedure is possible because in Section 3.2 we will match the expression for the NNLO cross section in NRQCD directly to the corresponding two-loop expression in full QCD. As a consequence additional constant terms in the brackets on the RHS of Eq. (30) do not affect the final result for the cross section at NNLO in NRQCD because they merely represent contributions which can be anyway freely shifted between the nonrelativistic correlators and the short-distance coefficients. The resulting (small) ambiguity will be accounted for during the fitting procedure by varying the factorization scale $\mu_{\rm fac}$. However, the reader should note that even with a more stringent regularization scheme like the $\overline{\rm MS}$ scheme this ambiguity cannot be avoided because the factorization $\mu_{\rm fac}$ is by construction not fixed to any

value regardless which regularization scheme is used.[7] For later reference we call $G_c^{(0),\,reg}(0,0,E)$ "zero-distance Coulomb Green function". A graphical representation of $G_c^{(0),\,reg}(0,0,E)$ in terms of NRQCD Feynman diagrams is displayed in Fig. 7a. For convenience we suppress the superscript "reg" from now in this work.

The Coulomb Green function contains $b\bar{b}$ bound state poles at the energies $\sqrt{s}_n = 2M_b - C_F^2 a_s^2 M_b/4n^2$ $(n = 1, 2, \ldots \infty)$. These poles come from the digamma function in Eq. (31) and correspond to the nonrelativistic positronium state poles known from QED [29]. They are located entirely *below* the threshold point $\sqrt{s}_{\rm thr} = 2M_b$. This can be seen explicitly from the cross section in the nonrelativistic limit,

$$\begin{aligned} R_{\rm LO}^{\rm thr} &= \frac{\pi\, Q_b^2}{M_b^2}\,{\rm Im}\Big[\,\mathcal{A}_1\,\Big]^{\rm LO} = \frac{6\,\pi\, N_c\, Q_b^2}{M_b^2}\,{\rm Im}\Big[\,G_c^{(0)}(0,0,E)\,\Big] \\ &= \frac{24\,\pi^2\, N_c\, Q_b^2}{M_b}\,\sum_{n=1}^{\infty}\,|\Psi_n(0)|^2\,\delta(s-s_n) \,+\, \Theta(E)\,\frac{3}{2}\,N_c\,Q_b^2\,\frac{C_F\,a_s\,\pi}{1-\exp(-\frac{C_F\,a_s\,\pi}{v})}\,, \end{aligned} \tag{32}$$

where $|\Psi_n(0)|^2 = (M_b C_F a_s)^3/8\pi n^3$ is the modulus squared of the LO nonrelativistic bound state wave functions for the radial quantum number n. The continuum contribution on the RHS of Eq. (32) is sometimes called "Sommerfeld factor" of "Fermi factor" in the literature. The resonance contributions are described by the first term in the second line of Eq. (32). The corrections to the zero-distance Coulomb Green function calculated below lead to higher order contributions to the bound state energy levels, the residues at the bound state poles and the continuum. We would like to stress that all these contributions must be included in the dispersion integration (4) to arrive at reliable results for the theoretical moments P_n^{th}. Nevertheless, it is worth to note that the resonances are not necessarily equivalent to the actual Υ resonances [5]. In particular for large radial excitations a direct comparison would be more than suspicious. In the context of the calculation of the moments they have to be included for mathematical rather than physical reasons. (See also the discussion in Section 4.)

Let us now come to the determination of the corrections to the zero-distance Coulomb Green function coming from the remaining terms in the Schrödinger equation (24). At NLO only the one-loop contributions to the Coulomb potential, $V_c^{(1)}$ (see Eq. (19)), have to considered. Using first order TIPT in configuration space representation the NLO corrections to $G_c^{(0)}(0,0,E)$ read

$$G_c^{(1)}(0,0,E) \;=\; -\int d^3\vec{r}\, G_c^{(0)}(0,r,E)\, V_c^{(1)}(\vec{r})\, G_c^{(0)}(r,0,E)\,. \tag{33}$$

Expression (33) is displayed graphically in Fig. 7b. Further evaluation of the integration on the RHS of Eq (33) is possible but not presented here, because it is already in a form suitable for the dispersion integration (4) (see Section 3.3). At NNLO several contributions have to be considered. The corrections from the two-loop contributions to the Coulomb potential, $V_c^{(2)}$ (see Eq. (22)), are calculated in analogy to the NLO contributions using first order TIPT (Fig. 7c)

$$\Big[\,G_c^{(2)}(0,0,E)\,\Big]_c^{2\,\rm loop} \;=\; -\int d^3\vec{r}\, G_c^{(0)}(0,r,E)\, V_c^{(2)}(\vec{r})\, G_c^{(0)}(r,0,E)\,. \tag{34}$$

We also have to take into account the one-loop Coulomb potential (Fig. 7(d)) in second order TIPT,

$$\Big[\,G_c^{(2)}(0,0,E)\,\Big]_c^{1\,\rm loop} =$$

[7] In fact, using the $\overline{\rm MS}$ scheme is a quite tricky (but not impossible) task if one wants to avoid solving the Schrödinger equation in D dimensions.

$$= \int d^3\vec{r}_1 \int d^3\vec{r}_2\, G_c^{(0)}(0,r_1,E)\, V_c^{(1)}(\vec{r}_1)\, G_c^{(0),S}(\vec{r}_1,\vec{r}_2,E)\, V_c^{(1)}(\vec{r}_2)\, G_c^{(0)}(r_2,0,E)\,. \qquad (35)$$

Because the Coulomb potential is angular independent, only the S-wave components of the Coulomb Green function in the center of expression (35) are needed. Finally, we have to determine the NNLO contributions to the zero-distance Green function coming from the kinetic energy, $\delta H_{\rm kin} = -\vec{\nabla}^4/4M_b^3$, the Breit-Fermi potential $V_{\rm BF}$ and the non-Abelian potential $V_{\rm NA}$ (see Figs. 7e and f). These corrections are symbolized by $[G_c^{(2)}(0,0,E)]^{\rm kin+BF+NA}$ in the following. A method to determine them has been presented in an earlier publication [7, 10]. Some details about this method are presented in Appendix A. The final result for $[G_c^{(2)}(0,0,E)]^{\rm kin+BF+NA}$ reads

$$\begin{aligned} &G_c^{(0)}(0,0,E) + \Big[\, G_c^{(2)}(0,0,E)\,\Big]^{\rm kin+BF+NA} \;= \\ &= \frac{M_b^2}{4\,\pi}\left\{ i\,v\left(1+\frac{5}{8}\,v^2\right) - C_F\,a_s\left(1+2\,v^2\right)\left[\,\ln(-i\frac{M_b\,v}{\mu_{\rm fac}}) + \gamma_{\rm E} + \Psi\!\left(1 - i\,\frac{C_F\,a_s\,(1+\frac{11}{8}v^2)}{2\,v}\right)\right]\right\} \\ &\quad + \frac{C_F\,a_s\,M_b^2}{12\,\pi}\left(1+\frac{3}{2}\,\frac{C_A}{C_F}\right)\left\{\, i\,v - C_F\,a_s\left[\,\ln(-i\frac{M_b\,v}{\mu_{\rm fac}}) + \gamma_{\rm E} + \Psi\!\left(1 - i\,\frac{C_F\,a_s}{2\,v}\right)\right]\right\}^2 . \end{aligned} \qquad (36)$$

Because $[G_c^{(2)}(0,0,E)]^{\rm kin+BF+NA}$ contains also kinematic corrections to the zero-distance Coulomb Green function, we found it convenient to add the zero-distance Coulomb Green function (31). The first term on the RHS of Eq. (36) represents the zero-distance Coulomb Green function including the NNLO kinematic corrections and the second term the remaining corrections. It is an interesting fact that these remaining corrections can be written as the squared of the zero-distance Coulomb Green function. This is a consequence of the (renormalization group) invariance of the total cross section (13) under variations of the factorization scale $\mu_{\rm soft}$. (See also the comment after Eq. (64).) Collecting all contributions the complete expression for the nonrelativistic correlator $\mathcal{A}_1$ at NNLO reads

$$\begin{aligned} \mathcal{A}_1 \;=\; & 6\,N_c\left\{ G_c^{(0)}(0,0,E) + G_c^{(1)}(0,0,E)\right. \\ & \left. + \Big[\, G_c^{(2)}(0,0,E)\,\Big]_c^{1\,\rm loop} + \Big[\, G_c^{(2)}(0,0,E)\,\Big]_c^{2\,\rm loop} + \Big[\, G_c^{(2)}(0,0,E)\,\Big]^{\rm kin+BF+NA}\right\}. \end{aligned} \qquad (37)$$

The calculation of the correlator $\mathcal{A}_2$, on the other hand is trivial using the equation of motion for the Green function, see Eq. (16). Because $\mathcal{A}_2$ is multiplied by an explicit factor v^2, Eq. (16), its form is particularly simple,

$$\mathcal{A}_2 \;=\; v^2\,\frac{3\,M_b^4}{2\,\pi}\left\{\, i\,v - C_F\,a_s\left[\,\ln\Big(-i\frac{M_b\,v}{\mu_{\rm fac}}\Big) + \gamma_{\rm E} + \Psi\Big(1 - i\,\frac{C_F\,a_s}{2\,v}\Big)\right]\right\}. \qquad (38)$$

3.2 Determination of the Short-distance Coefficients

The short-distance coefficient C_1 and C_2 are determined by matching the NNLO cross section (13) in NRQCD to the same cross section calculated in full QCD (in the limit $\alpha_s \ll v \ll 1$) at the two-loop level and including terms in the velocity expansion up to NNLO. It is convenient to parameterize the higher order contributions to C_1 in the form ($a_h \equiv \alpha_s(\mu_{\rm hard})$)

$$C_1(M_b,\mu_{\rm hard},\mu_{\rm fac}) \;=\; 1 + \Big(\frac{a_h}{\pi}\Big)\,c_1^{(1)} + \Big(\frac{a_h}{\pi}\Big)^2\,c_1^{(2)}(\mu_{\rm hard},\mu_{\rm fac}) + \ldots\,. \qquad (39)$$

Due to renormalization group invariance only the $\mathcal{O}(\alpha_s^2)$ coefficient of C_1 depends on the hard scale $\mu_{\rm hard}$. We have already anticipated that the $\mathcal{O}(\alpha_s)$ coefficient does not depend on the factorization scale $\mu_{\rm fac}$. For C_2, on the other hand, no higher order contributions are needed because the correlator $\mathcal{A}_2$ is already of NNLO,

$$C_2 \,=\, 1\,. \tag{40}$$

The expansion of the NNLO cross section in NRQCD, $R^{\rm thr}_{\rm NNLO}$, Eq. (13), keeping terms up to order α_s^2, reads

$$\begin{aligned}
R^{\rm thr}_{\rm NNLO} \;&\stackrel{\alpha_s\ll 1}{=}\; N_c\, Q_b^2 \left\{ \left[\frac{3}{2}\, v - \frac{17}{16}\, v^3 \right] + \frac{C_F\, a_h}{\pi} \left[\frac{3\,\pi^2}{4} - 6\, v + \frac{\pi^2}{2}\, v^2 \right] \right. \\
&+ a_h^2 \left[\frac{C_F^2\,\pi^2}{8\, v} + \frac{3}{2} C_F \left(-2\, C_F + C_A \Big(-\frac{11}{24} \ln \frac{4\, v^2 M_t^2}{\mu_{\rm hard}^2} + \frac{31}{72} \Big) + T\, n_l \Big(\frac{1}{6} \ln \frac{4\, v^2 M_t^2}{\mu_{\rm hard}^2} - \frac{5}{18} \Big) \right) \right. \\
&\left. \left. + \Big(\frac{49\, C_F^2\, \pi^2}{192} + \frac{3}{2}\, \frac{c_1^{(2)}}{\pi^2} - C_F \Big(C_F + \frac{3}{2}\, C_A \Big) \ln \frac{M_b\, v}{\mu_{\rm fac}} \Big)\, v \right] + \mathcal{O}(\alpha_s^3) \right\}. \qquad (41)
\end{aligned}$$

where we have set $\mu_{\rm soft} = \mu_{\rm hard}$ because in the limit $\alpha_s \ll v \ll 1$ a distinction between soft and hard scale is irrelevant. (We want to emphasize that the choice $\mu_{\rm soft} = \mu_{\rm hard}$ implicitly means that the hard scale is, like the soft scale, defined in the $\overline{\rm MS}$ scheme.) The corresponding expression for the two-loop cross section calculated in full QCD reads[8]

$$\begin{aligned}
R^{\rm NNLO}_{\rm 2loop\ QCD} \;&\stackrel{v\ll 1}{=}\; N_c\, Q_b^2 \left\{ \left[\frac{3}{2}\, v - \frac{17}{16}\, v^3 + \mathcal{O}(v^4) \right] + \frac{C_F\, a_h}{\pi} \left[\frac{3\,\pi^2}{4} - 6\, v + \frac{\pi^2}{2}\, v^2 + \mathcal{O}(v^3) \right] \right. \qquad (42) \\
&+ a_h^2 \left[\frac{C_F^2\,\pi^2}{8\, v} + \frac{3}{2} C_F \left(-2\, C_F + C_A \Big(-\frac{11}{24} \ln \frac{4\, v^2 M_t^2}{\mu_{\rm hard}^2} + \frac{31}{72} \Big) + T\, n_l \Big(\frac{1}{6} \ln \frac{4\, v^2 M_t^2}{\mu_{\rm hard}^2} - \frac{5}{18} \Big) \right) \right. \\
&\left. \left. + \Big(\frac{49\, C_F^2\, \pi^2}{192} + \frac{3}{2}\, \kappa + \frac{C_F}{\pi^2} \Big(\frac{11}{2}\, C_A - 2\, T\, n_l \Big) \ln \frac{M_t^2}{\mu_{\rm hard}^2} - C_F \Big(C_F + \frac{3}{2}\, C_A \Big) \ln v \Big)\, v \right] + \mathcal{O}(v^2) \right\},
\end{aligned}$$

where

$$\begin{aligned}
\kappa \;&=\; C_F^2 \left[\frac{1}{\pi^2} \left(\frac{39}{4} - \zeta_3 \right) + \frac{4}{3} \ln 2 - \frac{35}{18} \right] \\
&\quad - C_A\, C_F \left[\frac{1}{\pi^2} \left(\frac{151}{36} + \frac{13}{2} \zeta_3 \right) + \frac{8}{3} \ln 2 - \frac{179}{72} \right] \\
&\quad + C_F\, T \left[\frac{4}{9} \left(\frac{11}{\pi^2} - 1 \right) \right] + C_F\, T\, n_l \left[\frac{11}{9\,\pi^2} \right]. \qquad (43)
\end{aligned}$$

The Born and one-loop contributions in Eq. (42) are standard [30, 31]. The two-loop contributions are presented with the various combinations of the SU(3) group theoretical factors $C_F = 4/3$, $C_A = 3$ and $T = 1/2$. The terms proportional to C_F^2 come from the QED-like, Abelian exchange of two gluons and have been calculated analytically in [32]. The result has been confirmed numerically in [33] and analytically in [34, 35]. The corresponding Feynman diagrams (in the covariant gauge) are displayed in Fig. 8(a), (b), (c) and (d). The $C_A C_F$ terms correspond to the non-Abelian exchange of two gluons,

[8] The two-loop contributions from secondary radiation of a $b\bar{b}$ pair off a light quark-antiquark pair are kinematically suppressed and do not contribute at NNLO in the velocity expansion.

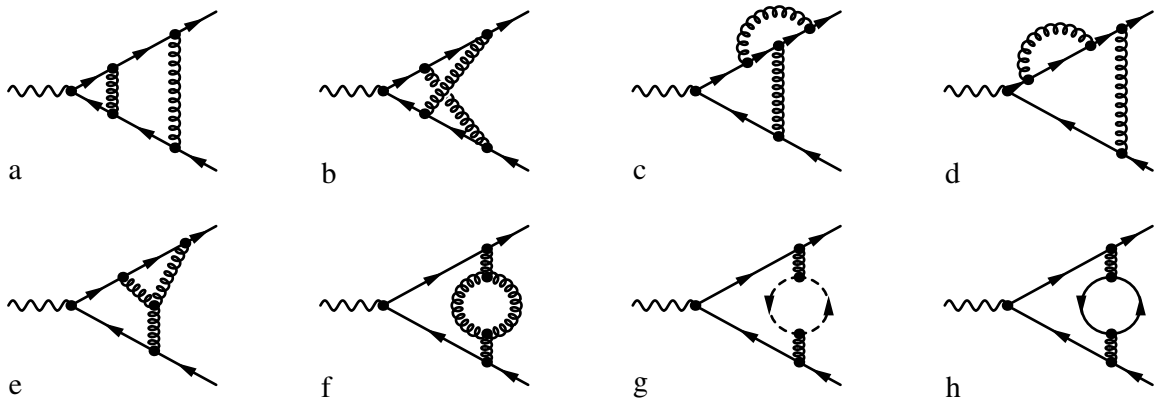

Figure 8: QCD Feynman diagrams relevant for the calculation of the cross section at the two-loop level. The calculation of these diagrams is needed for the matching calculation which leads to the determination of the short-distance coefficient C_1. Feynman diagrams needed for the wave function renormalization are not displayed.

i.e. involving the triple gluon vertex, ghost fields and topologies with crossed gluon lines (Figs. 8(b), (c), (d), (e), (f), (g)). These contributions have been determined in [34, 35]. The $C_F T n_l$ contributions are from diagrams with a vacuum polarization of massless quarks (Fig. 8(h)) and have been calculated in [36]. The contributions proportional to $C_F T$, finally, correspond to the diagram where the vacuum polarization is from the bottom quarks (Fig. 8(g)) and have been calculated in [37, 36]. The virtual top quark contributions are suppressed by a factor $(M_b/M_t)^2 \sim 0.001$) and are neglected.

The constants $c_1^{(1)}$ and $c_1^{(2)}$ defined in Eq. (39) can now be easily determined by demanding equality of expressions (41) and (42). This constitutes the "direct matching" procedure [7, 16] and leads to

$$c_1^{(1)} = -4\,C_F\,, \tag{44}$$

$$c_1^{(2)} = \pi^2 \left[\kappa + \frac{C_F}{\pi^2} \left(\frac{11}{3}\,C_A - \frac{4}{3}\,T\,n_l \right) \ln \frac{M_b^2}{\mu_{\rm hard}^2} + C_F \left(\frac{1}{3}\,C_F + \frac{1}{2}\,C_A \right) \ln \frac{M_b^2}{\mu_{\rm fac}^2} \right]. \tag{45}$$

The constant $c_1^{(1)}$ is the $\mathcal{O}(\alpha_s)$ short-distance contributions which is well known from the single photon annihilation contributions to the positronium hyperfine splitting [38] and from corrections to electromagnetic quarkonium decays [39]. We want to mention again that $\mu_{\rm hard}$ and $\mu_{\rm fac}$ are independent and defined in different regularization schemes.

To conclude this subsection we would like to point out that the short-distance coefficients C_1 and C_2 determined above are not sufficient to determine the vacuum polarization function (Eq. (1)) in the threshold regime at NNLO, because they have been determined via matching at the level of the cross section only, i.e. at the level of the imaginary part of the vacuum polarization function. The expressions for the correlators still contain overall UV divergences $\propto \ln(M_b/\mu_{\rm fac})$ in their real parts [19, 29], see e.g. Eq. (31). For the large n moments calculated in this work these ambiguities are irrelevant because the divergent contributions in the real parts do not contribute to the large n moments. The relation between the nonrelativistic correlators and the vacuum polarization function

at NNLO in the threshold regime, including the proper short-distance contributions for the real part, has the form

$$\begin{aligned}
&\frac{1}{3\,q^2}\,\Pi^\mu_\mu(q) \stackrel{q^2\to 4M_b^2}{\longrightarrow} \\
&\quad \frac{1}{12\,M_b^2}\,C_1(\mu_{\rm hard},\mu_{\rm fac})\,\mathcal{A}_1(E,\mu_{\rm soft},\mu_{\rm fac}) - \frac{1}{9M_b^4}\,C_2(\mu_{\rm hard},\mu_{\rm fac})\,\mathcal{A}_2(E,\mu_{\rm soft},\mu_{\rm fac}) + \ldots \\
&\quad + h_1 + \frac{C_F\,a_h}{4\,\pi}\left[\frac{1}{2}\,\ln\Big(\frac{M_b}{\mu_{\rm fac}}\Big) + h_2\right] + \ldots\,. \qquad (46)
\end{aligned}$$

The constants h_1 and h_2 can be determined via (direct) matching to the one and two-loop vacuum polarization function in full QCD at threshold, i.e. for $q^2 \to 4M_b^2$. This work has been carried out in a previous publication [16] and leads to $h_1 = \frac{2}{9\pi^2}$ and $h_2 = \frac{1}{4\pi^2}(3 - \frac{21}{2}\zeta_3) + \frac{11}{32} - \frac{3}{4}\ln 2$. For the complete expression of the vacuum polarization function in the threshold regime at NNLO in the nonrelativistic expansion also the $\mathcal{O}(\alpha_s^2)$ and $\mathcal{O}(\alpha_s^3)$ short-distance contributions would have to be calculated. This would require the calculation of the three- and four loop the vacuum polarization functions in full QCD in the threshold regime. This task has not been accomplished yet and remains to be done.[9]

3.3 The Dispersion Integration

After the nonrelativistic correlators $\mathcal{A}_1$ and $\mathcal{A}_2$ and the short-distance constants C_1 and C_2 are calculated we are now ready to carry out the dispersion integration (4). This task is quite cumbersome if the complete covariant form of the integration measure ds/s^{n+1} is used. Fortunately the integration can be simplified because we are only interested in NNLO accuracy in the nonrelativistic expansion in $v = (E/M_b)^{1/2}$. Changing the integration variable to the energy $E = \sqrt{s} - 2M_b$ and expanding up to NNLO in v, where combination $(E/M_b)n$ is considered of order one, the resulting integration measure reads

$$\begin{aligned}
\frac{ds}{s^{n+1}} \quad &= \quad \frac{1}{(4\,M_b^2)^n}\,\frac{dE}{M_b}\,\exp\left\{-(2\,n+1)\,\ln\Big(1+\frac{E}{2\,M_b}\Big)\right\} \\
&\stackrel{E\ll M_b}{\longrightarrow} \quad \frac{1}{(4\,M_b^2)^n}\,\frac{dE}{M_b}\,\exp\left\{-\frac{E}{M_b}\,n\right\}\left(1-\frac{E}{2\,M_b}+\frac{E^2}{4\,M_b^2}\,n+\mathcal{O}\Big(\frac{E^2}{M_b^2},\frac{E^3}{M_b^3}\,n,\frac{E^4}{M_b^4}\,n^2\Big)\right). \qquad (47)
\end{aligned}$$

The dispersion integration for the theoretical moments P_n^{th} at NNLO then takes the form

$$P_n^{th} \;=\; \frac{1}{(4\,M_b^2)^n}\int\limits_{E_{\rm bind}}^{\infty}\frac{dE}{M_b}\,\exp\left\{-\frac{E}{M_b}\,n\right\}\left(1-\frac{E}{2\,M_b}+\frac{E^2}{4\,M_b^2}\,n\right)R^{\rm thr}_{\rm NNLO}(E)\,, \qquad (48)$$

where $E_{\rm bind}$ is the (negative) binding energy of the lowest lying resonance. We would like to point out that expansion (47) leads to an asymptotic series, which means that including more an more terms in the expansion can improve the approximation only up to a certain point beyond which the series

[9] In Refs. [40] numerical approximations for the three loop vacuum polarization valid for all energies has been obtained based on the Padé method. Unfortunately numerical approximations are of little use for a precise extraction the $\mathcal{O}(\alpha_s^2)$ short-distance constants due to the presence of singular terms $\propto \ln v$ and $\ln^2 v$ in the real part of the three loop vacuum polarization function close to the threshold.

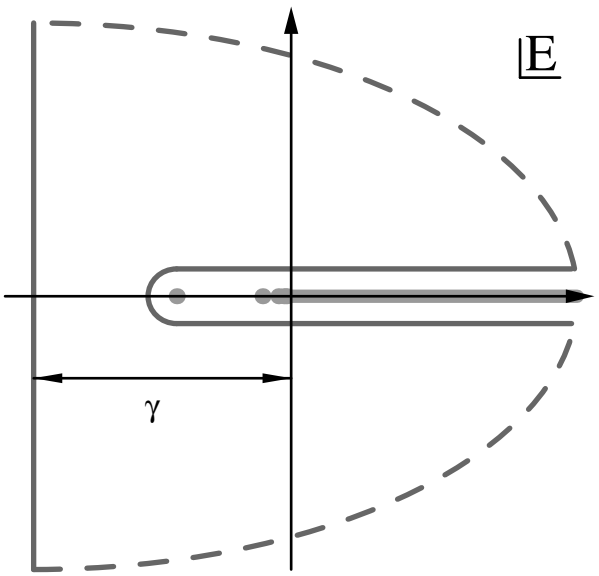

Figure 9: Path of integration to calculate expression (48) for the theoretical moments P_n^{th}. The dashed line closes the contour at infinity and does not contribute to the integration. The constant γ is chosen large enough to be safely away from the bound state poles which are indicated by the gray dots on the negative energy axis. The thick gray line on the positive energy axis represents the continuum.

starts diverging. We have checked that for all values of n employed in this work the expansion is still well inside the converging regime. It should also be noted that for increasing values of n the expansion provides better and better approximations only as long as the condition $(E_{\rm bind}/M_b)n < 1$ is satisfied. In our case, where the $b\bar{b}$ system is treated as Coulombic, i.e. $E_{\rm bind} = M_b C_F^2 \alpha_s^2/4 + \ldots$. this condition is always satisfied. (See also discussion at the end of Section 4.) Integration (48) is carried out most efficiently by deforming the path of integration into the negative complex energy plane as shown in Fig. 9. Because the (dashed) line which closes the contour at infinity does not contribute and because we take γ large enough to be safely away from the bound state poles ($\gamma \gg E_{\rm bind}$), we can rewrite expression (48) as

$$
\begin{aligned}
P_n^{th} &= \frac{-2\,i\,Q_b^2\,\pi}{(4M_b^2)^{n+1}} \int\limits_{-\gamma-i\infty}^{-\gamma+i\infty} \frac{dE}{M_b} \exp\left\{ -\frac{E}{M_b} n \right\} \left(1 - \frac{E}{2M_b} + \frac{E^2}{4M_b^2} n \right) \left[C_1 \mathcal{A}_1(E) - \frac{4}{3M_b^2} C_2 \mathcal{A}_2(E) \right] \\
&= \frac{4Q_b^2\pi^2}{(4M_b^2)^{n+1}} \frac{1}{2\pi i} \int\limits_{\gamma-i\infty}^{\gamma+i\infty} \frac{d\tilde{E}}{M_b} \exp\left\{ \frac{\tilde{E}}{M_b} n \right\} \left(1 + \frac{\tilde{E}}{2M_b} + \frac{\tilde{E}^2}{4M_b^2}\, n \right) \left[C_1\, \mathcal{A}_1(-\tilde{E}) - \frac{4}{3M_b^2}\, C_2\, \mathcal{A}_2(-\tilde{E}) \right],
\end{aligned}
\tag{49}
$$

where in second line the change of variables $E \to -\tilde{E}$ has been performed. The reader should note that for the integration in the negative complex energy plane also the real part of the correlators $\mathcal{A}_1$

and $\mathcal{A}_2$ is needed. The expression in the second line of Eq. (49) offers three advantages which make it much easier to calculate than expression (48):

1. Because the integration path is far away from bound state energies, the integrand can be expanded in α_s. This avoids that we have to integrate over complicated special function like the digamma function Ψ.

2. We do not have to integrate separately over the resonances and the continuum. Both contributions are in a convenient way calculated at the same time.

3. The expression in the second line of Eq. (49) is nothing else than an inverse Laplace transform for which a vast number of tables exist in literature (see e.g. [28]).

We want to stress that the advantages described above are merely technical in nature and just simplify the calculation. The results of the integration are not affected.

The final result for the theoretical moments including all contributions up to NNLO in the nonrelativistic expansion can be cast into the form

$$P_n^{th} \;=\; \frac{3\,N_c\,Q_b^2\,\sqrt{\pi}}{4\,(4\,M_b^2)^n\,n^{3/2}} \left\{ C_1(\mu_{\rm hard},\mu_{\rm fac})\,\varrho_{n,1}(\mu_{\rm soft},\mu_{\rm fac}) + C_2\,\varrho_{n,2} \right\} \tag{50}$$

where $\varrho_{n,1}$ comes from the integration of the correlator $\mathcal{A}_1$ (including LO, NLO and NNLO contributions in the nonrelativistic expansion) and $\varrho_{n,2}$ originate from the integration of $\mathcal{A}_2$ which is of NNLO only. To illustrate the technical aspects of the integration (49) let first present some of the details of the calculation of the LO contribution to $\varrho_{n,1}$. The LO contributions to $\varrho_{n,1}$ originates from the zero-distance Coulomb Green function in Eq. (31). The corresponding integration takes the form

$$\begin{aligned}
\Big[\,\varrho_{n,1}\,\Big]^{\rm LO} &= \frac{8\,\pi^{3/2}\,n^{3/2}}{M_b^2}\,\frac{1}{2\,\pi\,i}\int\limits_{\gamma-i\infty}^{\gamma+i\infty}\frac{d\tilde{E}}{M_b}\,\exp\left\{\frac{\tilde{E}}{M_b}\,n\right\}G_c^{(0)}(0,0,-\tilde{E}) \\
&= 2\,\sqrt{\pi}\,n^{3/2}\,\frac{1}{2\,\pi\,i}\int\limits_{\gamma-i\infty}^{\gamma+i\infty}\frac{d\tilde{E}}{M_b}\,\exp\left\{\frac{\tilde{E}}{M_b}\,n\right\}\Big[\,-\tilde{v}-C_F\,a_s\,\ln\tilde{v}+C_F\,a_s\sum_{p=2}^{\infty}\zeta_p\left(\frac{C_F\,a_s}{2\,\tilde{v}}\right)\Big]\,,
\end{aligned} \tag{51}$$

where

$$\tilde{v}\;\equiv\;\sqrt{\frac{\tilde{E}}{M_b}} \tag{52}$$

and ζ_p is the Riemann zeta function for the argument p. Because $|C_F a_s/2\tilde{v}| \ll 1$ along the integration path we have expanded the digamma function in $G_c^{(0)}(0,0,-\tilde{E})$ for small α_s. The resulting expression is now immediately ready for the application of inverse Laplace transforms. Here, we only need the relations

$$\begin{aligned}
\frac{1}{2\pi i}\int\limits_{\gamma-i\infty}^{\gamma+i\infty}\frac{1}{x^\nu}\,e^{x\,t}\,dx &= \frac{t^{\nu-1}}{\Gamma(\nu)}\,, \\
\frac{1}{2\pi i}\int\limits_{\gamma-i\infty}^{\gamma+i\infty}\frac{\ln x}{x^\nu}\,e^{x\,t}\,dx &= \frac{t^{\nu-1}}{\Gamma(\nu)}\Big[\,\Psi(\nu)-\ln t\,\Big]\,.
\end{aligned} \tag{53}$$

The result for $[\varrho_{n,1}]^{\rm LO}$ reads

$$\Big[\,\varrho_{n,1}\,\Big]^{\rm LO} \;=\; 1 + 2\,\sqrt{\pi}\,\phi + 4\,\sqrt{\pi}\,\sum_{p=2}^{\infty}\,\phi^p\,\frac{\zeta_p}{\Gamma(\frac{p-1}{2})} \tag{54}$$

where

$$\phi \;\equiv\; \frac{C_F\,a_s\,\sqrt{n}}{2}\,. \tag{55}$$

Expression (54) can be rewritten in the form

$$\Big[\,\varrho_{n,1}\,\Big]^{\rm LO} \;=\; 1 + 2\,\sqrt{\pi}\,\phi + \frac{2\,\pi^2}{3}\,\phi^2 + 4\,\sqrt{\pi}\,\sum_{p=1}^{\infty}\,\left(\frac{\phi}{p}\right)^3\,\exp\left\{\left(\frac{\phi}{p}\right)^2\right\}\,\left[\,1 + {\rm erf}\Big(\frac{\phi}{p}\Big)\,\right] \tag{56}$$

where erf is the error function defined as ${\rm erf}(z) = \frac{2}{\sqrt{\pi}}\int_0^z \exp(-t^2)dt$. Expression (56) agrees with the result obtained by Voloshin [6]. The infinite series defined in Eq. (54) is absolute convergent with an infinite radius of convergence. For the values of n employed in this work ($4 \le n \le 10$), however, convergence is somewhat slow and a large number of terms have to be taken into account. This fact is

ϕ	0.5	0.6	0.7	0.8	0.9	1.0
$[\varrho_{n,1}]^{\rm LO}$	6.38	9.44	14.07	21.16	32.10	49.12
first three terms in Eq. (54)	4.42	5.50	6.71	8.05	9.52	11.12

Table 1: Comparison of the series for $[\varrho_{n,1}]^{\rm LO}$ with the sum of Born, one- and two-loop contributions in the series on the RHS of Eq. (54) for the values of ϕ employed in this work.

illustrated in Tab. 1 where the sum of the first three terms (corresponding to Born, one- and two-loop contributions) in the series (54) is compared to the total sum for values of ϕ between 0.5 and 1.0, which represent the range of ϕ values used in this work. Tab. 1 shows that the resummation of higher orders in α_s is essential to arrive at sensible results in particular for larger values of n. This feature remains true for all contributions to $\varrho_{n,1}$ and $\varrho_{n,2}$ and shows that a naive fixed order (multi-loop) calculation for the moments is unreliable for large values of n.

Along the lines of the calculation of $[\varrho_{n,1}]^{\rm LO}$ it is now straightforward to determine $\varrho_{n,2}$ and the NLO and NNLO contributions to $\varrho_{n,1}$. The contributions to $\varrho_{n,1}$ coming from the one- and two-loop corrections to the Coulomb potential, $V_c^{(1)}$ and $V_c^{(2)}$, have the form

$$\begin{aligned}
\Big[\,\varrho_{n,1}\,\Big]_c^{\rm NLO+NNLO} \;&=\; \frac{8\,\pi^{3/2}\,n^{3/2}}{M_b^2}\,\frac{1}{2\,\pi\,i}\int\limits_{\gamma-i\infty}^{\gamma+i\infty}\frac{d\tilde{E}}{M_b}\,\exp\left\{\frac{\tilde{E}}{M_b}\,n\right\}\,\Big\{\,G_c^{(1)}(0,0,-\tilde{E}) \\
&\qquad +\Big[\,G_c^{(2)}(0,0,-\tilde{E})\,\Big]_c^{1\ \rm loop} + \Big[\,G_c^{(2)}(0,0,-\tilde{E})\,\Big]_c^{2\ \rm loop}\,\Big\} \\
&=\; 4\,\sqrt{\pi}\,\delta_1\,\phi\,\Big\{\,\frac{1}{2}\,\ln\Big(\frac{\mu_1\,e^{\gamma_{\rm E}/2}\,\sqrt{n}}{2\,M_b}\Big) + \sum_{p=1}^{\infty}\,\phi^p\,\Big[\,w_p^1 + w_p^0\,{\rm cln}\Big(M_b, n, \frac{2}{\mu_1}, p\Big)\,\Big]\,\Big\} \\
&\quad +4\,\sqrt{\pi}\,\delta_2\,\phi\,\Big\{\,\frac{1}{2}\,\ln^2\Big(\frac{\mu_2\,e^{\gamma_{\rm E}/2}\,\sqrt{n}}{2\,M_b}\Big) + \frac{\pi^2}{16}
\end{aligned}$$

$$
\begin{aligned}
&+\sum_{p=1}^{\infty}\phi^p\left[\,w_p^2-2\,w_p^1\,\mathrm{cln}\Big(M_b,n,\frac{2}{\mu_2},p\Big)-w_p^0\,\mathrm{cln2}\Big(M_b,n,\frac{2}{\mu_2},p\Big)\,\right]\Bigg\}\\
&8\,\sqrt{\pi}\,\delta_3^2\,\phi^2\sum_{p=0}^{\infty}\phi^p\left[\,\tilde{w}_p^2\,\mathrm{csin}\Big(M_b,n,\frac{2}{\mu_3},\frac{\sqrt{n}}{M_b\,\pi\,\phi},p\Big)+\tilde{w}_p^1\,\mathrm{csinln}\Big(M_b,n,\frac{2}{\mu_3},\frac{\sqrt{n}}{M_b\,\pi\,\phi},p\Big)\right.\\
&\left.+\tilde{w}_p^0\,\mathrm{csinln2}\Big(M_b,n,\frac{2}{\mu_3},\frac{\sqrt{n}}{M_b\,\pi\,\phi},p\Big)\,\right], \qquad (57)
\end{aligned}
$$

where

$$
\begin{aligned}
\delta_1 &= \left(\frac{a_s}{4\,\pi}\right)2\,\beta_0+2\left(\frac{a_s}{4\,\pi}\right)^2\Big(\,2\,\beta_0\,a_1+\beta_1\,\Big),\\
\delta_2 &= \left(\frac{a_s}{4\,\pi}\right)^2 4\,\beta_0^2\,,\\
\delta_3 &= \left(\frac{a_s}{4\,\pi}\right)2\,\beta_0\,,\\
\mu_1 &= \mu_{\rm soft}\,\exp\left\{\,\frac{1}{\delta_1}\left[\left(\frac{a_s}{4\,\pi}\right)a_1+\left(\frac{a_s}{4\,\pi}\right)^2\Big(\,\frac{\pi^2}{3}\,\beta_0^2+a_2\,\Big)\right]\right\},\\
\mu_2 &= \mu_{\rm soft}\,,\\
\mu_3 &= \mu_{\rm soft}\,\exp\left(\,\frac{a_1}{2\,\beta_0}\,\right), \qquad (58)
\end{aligned}
$$

and

$$
\begin{aligned}
\mathrm{cln}(m,n,a,p) &\equiv \ln\Big(\frac{a\,m}{\sqrt{n}}\Big)+\frac{1}{2}\,\Psi\Big(\frac{p}{2}\Big), \qquad (59)\\
\mathrm{cln2}(m,n,a,p) &\equiv \left[\,\ln\Big(\frac{a\,m}{\sqrt{n}}\Big)+\frac{1}{2}\,\Psi\Big(\frac{p}{2}\Big)\,\right]^2-\frac{1}{4}\,\Psi'\Big(\frac{p}{2}\Big), \qquad (60)\\
\mathrm{csin}(m,n,a,b,p) &\equiv {}_0\mathrm{F}_2\Big(\frac{3}{2},\frac{\mathrm{p}+1}{2},-\frac{\mathrm{n}}{(2\,\mathrm{b}\,\mathrm{m})^2}\Big), \qquad (61)\\
\mathrm{csinln}(m,n,a,b,p) &\equiv \left[\,\ln\Big(\frac{a\,m}{\sqrt{n}}\Big)+\frac{1}{2}\,\Psi\Big(\frac{p+1}{2}\Big)\,\right]{}_0\mathrm{F}_2\Big(\frac{3}{2},\frac{\mathrm{p}+1}{2},-\frac{\mathrm{n}}{(2\,\mathrm{b}\,\mathrm{m})^2}\Big)\\
&\quad-\frac{d}{dp}\,{}_0\mathrm{F}_2\Big(\frac{3}{2},\frac{\mathrm{p}+1}{2},-\frac{\mathrm{n}}{(2\,\mathrm{b}\,\mathrm{m})^2}\Big), \qquad (62)\\
\mathrm{csinln2}(m,n,a,b,p) &\equiv \left\{\left[\,\ln\Big(\frac{a\,m}{\sqrt{n}}\Big)+\frac{1}{2}\,\Psi\Big(\frac{p+1}{2}\Big)\,\right]^2-\frac{1}{4}\,\Psi'\Big(\frac{p+1}{2}\Big)\right\}{}_0\mathrm{F}_2\Big(\frac{3}{2},\frac{\mathrm{p}+1}{2},-\frac{\mathrm{n}}{(2\,\mathrm{b}\,\mathrm{m})^2}\Big)\\
&\quad-2\left[\,\ln\Big(\frac{a\,m}{\sqrt{n}}\Big)+\frac{1}{2}\,\Psi\Big(\frac{p+1}{2}\Big)\,\right]\frac{d}{dp}\,{}_0\mathrm{F}_2\Big(\frac{3}{2},\frac{\mathrm{p}+1}{2},-\frac{\mathrm{n}}{(2\,\mathrm{b}\,\mathrm{m})^2}\Big)\\
&\quad+\frac{d^2}{dp^2}\,{}_0\mathrm{F}_2\Big(\frac{3}{2},\frac{\mathrm{p}+1}{2},-\frac{\mathrm{n}}{(2\,\mathrm{b}\,\mathrm{m})^2}\Big). \qquad (63)
\end{aligned}
$$

The coefficients of the beta function, $\beta_{0,1}$ and the constants $a_{1,2}$ are given in Eqs. (20) and (23). The function Ψ' is the derivative of the digamma function and ${}_0\mathrm{F}_2$ is a generalized hypergeometric

function [28]. The constants $w_p^{0,1,2}$ and $\tilde{w}_p^{0,1,2}$ are given in Appendix C. For the calculation of expression (57) the table of inverse Laplace transforms given in Appendix B has been used extensively. The term proportional to δ_1 in Eq. (57) contains the NLO contributions coming from $V_c^{(1)}$ and the NNLO contributions coming from the terms $\propto 1/r$ and $\propto \ln(\mu_{\rm soft}\, e_{\rm E}^{\gamma}\, r)/r$ in $V_c^{(2)}$ in first order TIPT. The term proportional to δ_2 contains the remaining NNLO corrections coming from the term $\propto \ln^2(\mu_{\rm soft}\, e_{\rm E}^{\gamma}\, r)/r$ in $V_c^{(2)}$. The expression proportional to δ_3, finally, arises from the second order interaction in TIPT of $V_c^{(1)}$. The NNLO contributions to $\varrho_{n,1}$ originating from the kinetic energy corrections, the Breit-Fermi potential, the non-Abelian potential (see Eq. (36) for the corresponding corrections to the zero-distance Green function) and the kinematic correction factor $(1 + \tilde{E}/2M_b + (\tilde{E}^2/4M_b^2)n)$ from Eq. (48) read

$$\begin{aligned}
&\Big[\,\varrho_{n,1}\,\Big]^{\rm LO} + \Big[\,\varrho_{n,1}\,\Big]^{\rm NNLO}_{\rm kin+BF+NA} = \\
&= \; 1 + \frac{9}{8\,n} + 2\,\sqrt{\pi}\,\phi\left[\,1 + \frac{2}{n}\,\right] + 4\,\sqrt{\pi}\sum_{p=2}^{\infty}\phi^p\,\frac{\zeta_p}{\Gamma(\frac{p-1}{2})}\left[\,1 + \frac{(3-p)\,(3+5\,p)}{8\,n}\,\right] \\
&\quad + \frac{8}{3\,n}\,\phi^2\left\{ -\left[\,1 - \frac{\gamma_{\rm E}}{2} - \ln(2\,\sqrt{n})\,\right] + 2\,\sqrt{\pi}\,\phi\left[\,\frac{\gamma_{\rm E}}{2} + \ln\sqrt{n}\,\right]\right. \\
&\qquad\quad -2\,\sqrt{\pi}\sum_{p=2}^{\infty}\frac{\phi^p}{\Gamma(\frac{p-1}{2})}\left[\,\zeta_p\left(\Psi\Big(\frac{p-1}{2}\Big) - 2\,\ln\sqrt{n}\right) + \zeta_{p+1}\,\right] \\
&\qquad\quad \left. +2\,\sqrt{\pi}\sum_{p,q=2}^{\infty}\phi^{p+q-1}\,\frac{\zeta_p\,\zeta_q}{\Gamma(\frac{p+q-2}{2})}\,\right\} \\
&\quad - \Big[\,\varrho_{n,1}\,\Big]^{\rm LO}\left[\,a_s^2\left(\,\frac{1}{3}\,C_F^2 + \frac{1}{2}\,C_A\,C_F\,\right)\,\ln\frac{M_b^2}{\mu_{\rm fac}^2}\,\right], \qquad (64)
\end{aligned}$$

where, for convenience, also the LO result from Eq. (54) has been added. From the last line of expression (64) one can easily determine a renormalization group equation (with respect to the factorization scale $\mu_{\rm fac}$) for $\varrho_{n,1}$ and $\varrho_{n,2}$, which would allow for a resummation of the corrections coming from the kinetic energy corrections, the Breit-Fermi potential and the non-Abelian potential to all orders in TIPT. Although it is quite tempting to carry out this resummation, we refrain from doing so because a resummation of those corrections would not account for the retardation effects mentioned in Section 2. The complete expression for $\varrho_{n,1}$ has the form

$$\varrho_{n,1} \;=\; \Big[\,\varrho_{n,1}\,\Big]^{\rm LO} + \Big[\,\varrho_{n,1}\,\Big]_{c}^{\rm NLO+NNLO} + \Big[\,\varrho_{n,1}\,\Big]^{\rm NNLO}_{\rm kin+BF+NA}. \qquad (65)$$

Finally, the result for $\varrho_{n,2}$ coming from the integration of $\mathcal{A}_2$, Eq. (38), reads

$$\varrho_{n,2} \;=\; \frac{1}{n}\left[\,-2 - \frac{8}{3}\,\sqrt{\pi}\,\phi + 4\,\sqrt{\pi}\sum_{p=2}^{\infty}\phi^p\,\frac{2\,(p-3)}{3}\,\frac{\zeta_p}{\Gamma(\frac{p-1}{2})}\,\right] \qquad (66)$$

From from expression (50) for the theoretical moments at NLO one can easily recover the moments at NNLO by setting

$$\begin{aligned}
C_1 &= 1 + \Big(\frac{a_h}{\pi}\Big)\,c_1^{(1)}\,, \\
C_2 &= 0\,,
\end{aligned}$$

Moment	$M_b/[GeV]$				$\alpha_s(M_z)$			
	4.6	4.8	5.0	5.2	0.10	0.11	0.12	0.13
$P_4^{th}/[10^{-xx}\,\mathrm{GeV}^{-8}]$	0.51	0.37	0.27	0.20	0.19	0.27	0.41	0.74
$P_6^{th}/[10^{-xx}\,\mathrm{GeV}^{-12}]$	0.67	0.41	0.25	0.16	0.17	0.26	0.46	0.97
$P_8^{th}/[10^{-xx}\,\mathrm{GeV}^{-16}]$	0.95	0.49	0.26	0.14	0.18	0.29	0.57	1.37
$P_{10}^{th}/[10^{-xx}\,\mathrm{GeV}^{-20}]$	1.42	0.61	0.27	0.13	0.19	0.34	0.73	1.99
$P_{20}^{th}/[10^{-xx}\,\mathrm{GeV}^{-40}]$	12.96	2.37	0.47	0.10	0.42	1.00	3.07	13.93
	$\alpha_s(M_z) = 0.118$				$M_b = 4.8$ GeV			
	$\mu_{\rm soft} = 2.5\,\mathrm{GeV}\,, \quad \mu_{\rm hard} = \mu_{\rm fac} = 5$ GeV							

Table 2: The theoretical moments P_n^{th} for $n = 4, 6, 8, 10, 20$ and fixed $\mu_{\rm soft} = 2.5$ GeV and $\mu_{\rm hard} = \mu_{\rm fac} = 5$ GeV for various values of M_b and $\alpha_s(M_z)$. The two-loop running for the strong coupling has been employed.

$$\begin{aligned} \delta_1 &= \left(\frac{a_s}{4\,\pi}\right) 2\,\beta_0\,, \\ \delta_2 &= \delta_3 \,=\, 0\,, \\ \mu_1 &= \mu_{\rm soft}\,\exp\left(\frac{a_1}{2\,\beta_0}\right), \end{aligned} \tag{67}$$

and by ignoring the corrections $[\varrho_{n,1}]^{\rm NNLO}_{\rm kin+BF+NA}$. The resulting expression for the NLO moments is identical to the one obtained by Voloshin [2].

4 Some Comments to the Moments

In this section we will spend some time to discuss some interesting properties of the theoretical moments P_n^{th} which have been calculated in Section 3. We will address three issues: (i) the relation between the strong dependence of the moments on M_b and α_s and the dependences of the moments on the scales $\mu_{\rm soft}$, $\mu_{\rm hard}$ and $\mu_{\rm fac}$, (ii) the properties of the resonance and continuum contributions and (iii) the quality of the nonrelativistic expansion.

It is a characteristic feature of the moments that they depend very strongly on the bottom quark mass M_b and the strong coupling α_s. This is illustrated in Tab. 2 where the moments P_n^{th} are displayed for $n = 4, 6, 8, 10, 20$ and for various values of M_b and $\alpha_s(M_z)$ while the renormalization scales are fixed to $\mu_{\rm soft} = 2.5$ GeV and $\mu_{\rm hard} = \mu_{\rm fac} = 5$ GeV. The dependence on M_b is powerlike ($P_n^{th} \sim M_b^{-2n}$) for dimensional reasons (see definition (3)). The dependence on α_s is exponentially (see e.g. Eq. (56)) and comes from the resummations of the ladder diagrams containing the exchange of longitudinal Coulomb gluons. At this point one might conclude that fitting the theoretical moments to the experimental ones would allow for an extremely precise extraction of M_b and α_s, in particular if n is chosen very large. Unfortunately this conclusion is wrong. It is wrong from the conceptual point of view because for increasing n the effective smearing range ΔE in the integral (4) becomes smaller

Moment	$\mu_{\rm soft}/[\text{GeV}]$			$\mu_{\rm hard}/[\text{GeV}]$			$\mu_{\rm fac}/[\text{GeV}]$		
	1.5	2.5	3.5	2.5	5.0	10.0	2.5	5.0	10.0
$P_4^{th}/[10^{-8}\,\text{GeV}^{-8}]$	0.94	0.37	0.27	0.31	0.37	0.43	0.45	0.37	0.25
$P_6^{th}/[10^{-12}\,\text{GeV}^{-12}]$	1.16	0.41	0.28	0.34	0.41	0.47	0.51	0.41	0.27
$P_8^{th}/[10^{-16}\,\text{GeV}^{-16}]$	1.53	0.49	0.33	0.41	0.49	0.56	0.62	0.49	0.32
$P_{10}^{th}/[10^{-20}\,\text{GeV}^{-20}]$	2.10	0.61	0.39	0.51	0.61	0.70	0.79	0.61	0.39
$P_{20}^{th}/[10^{-40}\,\text{GeV}^{-40}]$	11.89	2.37	1.28	1.98	2.37	2.72	3.17	2.37	1.47
	$\mu_{\rm hard} = 5$ GeV $\mu_{\rm fac} = 5$ GeV			$\mu_{\rm soft} = 2.5$ GeV $\mu_{\rm fac} = 5$ GeV			$\mu_{\rm soft} = 2.5$ GeV $\mu_{\rm hard} = 5$ GeV		

Table 3: The theoretical moments P_n^{th} for $n = 4, 6, 8, 10, 20$ and fixed $\alpha_s(M_z) = 0.118$ and $M_b = 4.8$ GeV for various choices of the renormalization scales $\mu_{\rm soft}$, $\mu_{\rm hard}$ and $\mu_{\rm fac}$. The two-loop running for the strong coupling has been employed.

and smaller, which makes the perturbative calculations for the moments become less trustworthy [14]. In Section 2 we have used this argument to determine an upper bound on the allowed values on n. However, besides the conceptual arguments, the perturbative series for the moments itself contains a mechanism which prevents an arbitrarily precise determination of M_b and α_s for large values of n. In Tab. 3 the theoretical moments P_n^{th}, $n = 4, 6, 8, 10, 20$, are displayed for different choices for $\mu_{\rm soft}$, $\mu_{\rm hard}$ and $\mu_{\rm fac}$ and for $\alpha_s(M_z) = 0.118$ and $M_b = 4.8$ GeV. It is obvious that the dependence of the moments on the renormalization scales, and in particular on the soft scale, is becoming increasingly strong for larger values of n. As an example, the moment P_{20}^{th} (P_{10}^{th}) can change by a factor of ten (five) if the soft scale is varied between 1.5 and 3.5 GeV. These huge scale dependences are mainly caused by the large NNLO contributions to the large n moments coming from the two-loop corrections to the Coulomb potential, $V_c^{(2)}$, the second iteration of one-loop corrections to the Coulomb potential, $V_c^{(1)}$, and the non-Abelian potential, $V_{\rm NA}$. During the fitting procedure, when all renormalization scales are scanned of the ranges (17), the large scale dependencies effectively compensate the strong dependence of the moments on M_b and α_s. In Section 6.1 it is shown that this affects mostly the extraction of α_s rendering the sum rule, at least at the present stage, a rather powerless tool as far as precision determinations of the strong coupling are concerned. We want to stress that this compensation represents a very delicate balance which, if at all, can only be trusted if n is not chosen too large. We believe that this balance is still under controll for the values of n used in this work ($4 \le n \le 10$), although no proof for this assumption can be given. However, it is certain that for even larger values of n the extracted values of M_b and α_s might contain sizable systematic errors.

We also would like to make one comment on the fact that the theoretical moments contain contributions from below ($E < 0$) and above ($E > 0$) the threshold point. As shown in Eq. (32), the former contributions come from the resonance poles whereas the latter arise from the continuum. To demonstrate the size of the resonance and the continuum contributions let us examine the LO contribution to $\varrho_{n,1}$ which respect to this aspect. The contributions to $[\varrho_{n,1}]^{\rm LO}$ from $E < 0$ and $E > 0$ can be calculated separately from Eq. (48) using the LO nonrelativistic expression for the cross section

ϕ	0.0	0.1	0.2	0.3	0.4	0.5	0.6	0.7	0.8	0.9	1.0
$[\varrho_{n,1}]^{\rm LO}_{E<0}$	0.00	0.02	0.14	0.50	1.25	2.65	5.05	9.01	15.42	25.66	42.00
$[\varrho_{n,1}]^{\rm LO}_{E>0}$	1.00	1.41	1.92	2.48	3.09	3.73	4.39	5.06	5.74	6.43	7.13

Table 4: The resonance ($E < 0$) and continuum ($E > 0$) contributions to the function $[\varrho_{n,1}]_{\rm LO}$ for $0.0 \leq \phi \leq 1.0$.

from Eq. (32), ($\phi = C_F\, a_s\, \sqrt{n}/2$)

$$\Big[\, \varrho_{n,1} \,\Big]^{\rm LO}_{E<0} \;=\; 8\,\sqrt{\pi} \sum_{p=1}^{\infty} \left(\frac{\phi}{p}\right)^3 \exp\left\{\left(\frac{\phi}{p}\right)^2\right\}, \tag{68}$$

$$\Big[\, \varrho_{n,1} \,\Big]^{\rm LO}_{E>0} \;=\; 1 + 2\,\sqrt{\pi}\,\phi + \frac{2\,\pi^2}{3}\,\phi^2 + 4\,\sqrt{\pi} \sum_{p=1}^{\infty} \left(\frac{\phi}{p}\right)^3 \exp\left\{\left(\frac{\phi}{p}\right)^2\right\} \left[\, -1 + {\rm erf}\left(\frac{\phi}{p}\right) \,\right]. \tag{69}$$

In Tab. 4 expressions (68) and (69) are evaluated for $0.0 \leq \phi \leq 1.0$. For $\phi \approx 0.5$ resonance and continuum contributions are approximately equal in size, whereas for larger values of ϕ the resonance contributions dominate. This shows explicitly that for large values of n (where $n > 4$ can already considered as large) the resonance effects cannot be neglected. In particular, any sum rule analysis which is based on the large n moments and ignores the resonance contributions will lead to a bottom quark mass which is too low. From Eq. (68) it is also conspicuous that there are no resonance contributions proportional to α_s^n with $n = 0, 1, 2$. This shows that in conventional multi-loop perturbation theory bound state contributions to the heavy-quark-antiquark production cross section (in lepton pair collisions) are produced by Feynman diagrams containing three and more loops. Because the two-loop level represents the current state of the art in covariant multi-loop calculations where the full quark mass and energy dependence is taken into account (see Ref. [41] for a review and [42] far a recent publications on this subject), these peculiar contributions to the cross section sitting below the threshold point have not been observed so far. At the three-loop level, however, the cross section *will* have singular contributions $\propto \alpha_s/v^2$ below the threshold. In fact, these contributions are required by the analyticity of the vacuum polarization function in the nonrelativistic regime. [Of course, for a proper description of the bound state regime fixed order multi-loop perturbation theory is insufficient and a resummation of the singular terms to all orders in α_s has to be carried out.]

Finally, we also would like to address the question how well the nonrelativistic (and asymptotic) expansion at NNLO for the cross section R (Eq. (5)) and the integration measure ds/s^{n+1} in the dispersion integral (4) can approximate a complete covariant calculation of the large n moments, where all mass and energy dependences would be accounted for exactly. Strictly speaking, this question cannot be answered entirely because a complete covariant calculation of the moments, Eq. (3), for large values of n is certainly an impossible task. (If it were possible, we would not use the nonrelativistic expansion and NRQCD in the first place.) However, a partial answer can be given by comparing the terms proportional to α_s^n with $n = 0, 1, 2$ in P_n^{th}, Eq. (50), to the corresponding contributions calculated in full QCD. For simplicity we only present a comparison of the Born and one-loop contributions in the following. The two-loop contributions lead to the same conclusions. The Born and the one-loop

contributions from P_n^{th} read

$$\Delta^{\rm Born}_{n,\rm NRQCD} \equiv \left\{ \left[\frac{3\,N_c\,Q_b^2\,\sqrt{\pi}}{4\,(4\,M_b^2)^n\,n^{3/2}} \right]^{-1} P_n^{th} \right\}^{\mathcal{O}(1)} = 1 - \frac{7}{8\,n}\,, \tag{70}$$

$$\begin{aligned}\Delta^{1\ \rm loop}_{n,\rm NRQCD} &\equiv \left\{ \left[\frac{3\,N_c\,Q_b^2\,\sqrt{\pi}}{4\,(4\,M_b^2)^n\,n^{3/2}} \left(\frac{C_F\,\alpha_s}{\pi}\right) \right]^{-1} P_n^{th} \right\}^{\mathcal{O}(\alpha_s)} \\ &= \pi^{3/2}\,\sqrt{n}\left(1+\frac{2}{3\,n}\right) - 4\left(1+\frac{9}{8\,n}\right). \end{aligned} \tag{71}$$

The complete covariant versions of expressions (70) and (71) in full QCD can be determined from the well known Born and one-loop formulae for the cross section [30, 31],

$$\begin{aligned} R^{\rm Born}(q^2) &= \frac{N_c\,Q_b^2}{2}\,\beta\,(3-\beta^2)\,, \\ R^{1\ \rm loop}(q^2) &= N_c\,Q_b^2\left(\frac{C_F\,\alpha_s}{\pi}\right)\left\{ \frac{3\,\beta\ (5-3\,\beta^2)}{8} \right. \\ &\quad - \beta\,(3-\beta^2)\left(2\,\ln(1-p)+\ln(1+p)\right) - \frac{(1-\beta)\ (33-39\,\beta-17\,\beta^2+7\,\beta^3)}{16}\,\ln p \\ &\quad \left. + \frac{(3-\beta^2)\ (1+\beta^2)}{2}\left[2\,{\rm Li}_2(p) + {\rm Li}_2(p^2) + \ln p\left(2\,\ln(1-p)+\ln(1+p)\right) \right] \right\}, \end{aligned} \tag{72}$$

where $\beta = (1-4M_b^2/q^2)^{1/2}$ and $p = (1-\beta)/(1+\beta)$ and $\rm Li_2$ is the dilogarithm, and the covariant form of the dispersion relation for the moments, Eq. (3),

$$\Delta^{\rm Born}_{n,\rm QCD} \equiv \left[\frac{3\,N_c\,Q_b^2\,\sqrt{\pi}}{4\,(4\,M_b^2)^n\,n^{3/2}} \right]^{-1} \int\limits_{4M_b^2}^{\infty} \frac{ds}{s^{n+1}}\,R^{\rm Born}(s)\,, \tag{73}$$

$$\Delta^{1\ \rm loop}_{n,\rm QCD} \equiv \left[\frac{3\,N_c\,Q_b^2\,\sqrt{\pi}}{4\,(4\,M_b^2)^n\,n^{3/2}} \left(\frac{C_F\,\alpha_s}{\pi}\right) \right]^{-1} \int\limits_{4M_b^2}^{\infty} \frac{ds}{s^{n+1}}\,R^{1\ \rm loop}(s)\,. \tag{74}$$

Expressions (73) and (74) can be easily calculated numerically. In Tab. 5 $\Delta^{\rm Born}_{n,\rm NRQCD}$, $\Delta^{\rm Born}_{n,\rm QCD}$, $\Delta^{1\ \rm loop}_{n,\rm NRQCD}$ and $\Delta^{1\ \rm loop}_{n,\rm QCD}$ are presented for $n = 1,\ldots,10$. The difference for the Born (one-loop) contributions amounts to 6% (7%) for $n = 4$ and quickly decreases for larger values of n. Thus, for the values of n employed in this work the asymptotic expansion in the velocity and, in particular, the use of NRQCD, lead to a sufficiently good approximation to the exact covariant results for the cases where a comparison can be carried out. [At this point one has to compare the quality of the approximation to the large scale variations of the moments discussed at the beginning of this section.] This strengthens our confidence that our method to calculate the theoretical moments is sufficient at the level of the remaining theoretical uncertainties. In particular, we cannot confirm the claims in [3] that the nonrelativistic expansion would behave badly and would represent a good approximation only for $n \sim 100$.

n	1	2	3	4	5	6	7	8	9	10
$\Delta^{\rm Born}_{n,\rm NRQCD}$	0.13	0.56	0.71	0.78	0.83	0.85	0.88	0.89	0.90	0.91
$\Delta^{\rm Born}_{n,\rm QCD}$	0.60	0.73	0.79	0.83	0.86	0.88	0.89	0.91	0.91	0.92
$\Delta^{\rm 1\ loop}_{n,\rm NRQCD}$	0.78	4.25	6.29	7.87	9.21	10.41	11.49	12.50	13.44	14.33
$\Delta^{\rm 1\ loop}_{n,\rm QCD}$	2.28	4.25	5.91	7.36	8.65	9.84	10.92	11.94	12.90	13.81

Table 5: The Born and one-loop contributions to the theoretical moments calculated in the nonrelativistic expansion (NRQCD) at NNLO and in full QCD for $n = 1, \ldots, 10$.

nS	$1S$	$2S$	$3S$
$M_{nS}/[\rm GeV]$	9.460	10.023	10.355
$\Gamma_{nS}/[\rm keV]$	$1.32 \pm 0.04 \pm 0.03$	$0.52 \pm 0.03 \pm 0.01$	$0.48 \pm 0.03 \pm 0.03$
nS	$4S$	$5S$	$6S$
$M_{nS}/[\rm GeV]$	10.58	10.87	11.02
$\Gamma_{nS}/[\rm keV]$	$0.25 \pm 0.03 \pm 0.01$	$0.31 \pm 0.05 \pm 0.07$	$0.13 \pm 0.03 \pm 0.03$
$\tilde{\alpha}^{-1}_{em} = \alpha^{-1}_{em}(10\ \rm GeV) = 131.8(1 \pm 0.005)\,, \quad (\sqrt{s})_{B\bar{B}} = 2 \times 5.279\ \rm GeV$			

Table 6: The Experimental number for the Υ masses and electronic decay widths used for the calculation of the experimental moments P^{ex}_n. For the widths the first error is statistical and the second systematic. The errors for Υ_{1S} and Υ_{2S} are taken from [43]. All the other errors are estimated from the numbers presented in [44]. The errors in the Υ masses and the $B\bar{B}$ threshold $(\sqrt{s})_{B\bar{B}}$ are neglected.

5 Experimental Moments the Fitting Procedure

In this section we will describe how the moments are calculated from experimental data and present our method to fit the experimental moments, P^{ex}_n, to the theoretical ones, P^{th}_n.

The experimental moments are determined using the available data on the Υ masses $M_{\Upsilon(nS)}$ and electronic partial widths $\Gamma_{\Upsilon(nS)} \equiv \Gamma(\Upsilon(nS) \to e^+e^-)$ for $n = 1, \ldots, 6$. For a compilation of all experimental numbers see Tab. 6. The formula for the experimental moments reads

$$P^{ex}_n \;=\; \frac{9\,\pi}{\tilde{\alpha}^2_{em}} \sum_{k=1}^{6} \frac{\Gamma_{kS}}{M^{2n+1}_{kS}} + \int\limits_{\sqrt{s}_{B\bar{B}}}^{\infty} \frac{ds}{s^{n+1}}\, r_{cont}(s)\,. \tag{75}$$

The first term on the RHS of Eq. (75) is obtained by using the narrow width approximation for all the known resonances

$$R_{res}(s) \;=\; \frac{9\,\pi}{\tilde{\alpha}^2_{em}} \sum_{n=1}^{\infty} \Gamma_{nS}\, M_{nS}\, \delta(s - M^2_{nS})\,. \tag{76}$$

$\tilde{\alpha}_{em}$ is the electromagnetic running coupling at the scale 10 GeV (see Tab. 6) which divides out the effects of the photonic vacuum polarization contained in the electromagnetic decay width.[10] The second term describes the contribution from the continuum above the $B\bar{B}$ threshold. We approximate the continuum cross section by a constant with a 50% error

$$r_{cont}(s) = r_c\,(1 \pm 0.5)\,. \tag{77}$$

This simplifies the treatment of experimental errors in the continuum regime significantly but also represents an reasonably good approximation because for $n \leq 4$ the continuum is already sufficiently suppressed that a more detailed description of it is not necessary. During the fitting procedure we vary the constant r_c between 0.5 and 1.5 which certainly covers all the experimental uncertainties. [In fact, this prescription renders the resonances $4S$, $5S$ and $6S$, which lie above the $B\bar{B}$ threshold practically irrelevant.]

For the fit we use the standard least squares method as described in [44]. The χ^2 function which has to be minimized reads

$$\chi^2(M_b, \alpha_s) \;=\; \sum_{\{n\},\{m\}} \left(P_n^{th} - P_n^{ex}\right) (S^{-1})_{nm} \left(P_m^{th} - P_m^{ex}\right). \tag{78}$$

$\{n\}$ represents the set of n's for which the fit shall be carried out and S^{-1} is the inverse covariance matrix describing the experimental errors and the correlation between the experimental moments. To construct the covariance matrix we use the errors in the electronic decay widths (where statistical and systematic errors are added quadratically), in the electromagnetic coupling $\tilde{\alpha}_{em}$ (see Tab. 6) and the error in the continuum cross section, Eq. (77), which we also treat as experimental. The tiny errors in the Υ masses are neglected. At this point it is important to note that the errors in the electronic widths are certainly not uncorrelated due to common sources of systematic errors in the e^+e^- collider experiments (mostly CLEO) where the widths have been determined. Unfortunately an analysis of these correlations cannot be found in the corresponding publications (see [44] for references). We therefore assume that the correlations between two widths can be written as

$$\overline{\delta\Gamma_{nS}\,\delta\Gamma_{mS}} \;=\; a_{cor}\,\delta\Gamma_{nS}^{sys}\,\delta\Gamma_{mS}^{sys}\,, \tag{79}$$

where $\delta\Gamma_{nS}$ is the systematic error in the electronic width Γ_{nS} as given in Tab. 6 and a_{cor} is a parameter which allow to switch the correlation on and off to check its impact on the extraction of M_b and α_s. During the fitting procedure a_{cor} is varied between zero (no correlation) and one (complete positive correlation of all systematic errors). Collecting all the quantities for which we take experimental errors into account into the vector

$$y_i \;=\; \left\{\Gamma_{1S}, \Gamma_{2S}, \Gamma_{3S}, \Gamma_{4S}, \Gamma_{5S}, \Gamma_{6S}, \tilde{\alpha}_{em}, r_{cont}\right\}, \qquad i = 1, \ldots, 8\,, \tag{80}$$

and using the standard error propagation formulae (see e.g. [44]) the covariance matrix reads

$$S_{nm} \;=\; \sum_{i,j=1}^{8} \left.\frac{\partial P_n^{ex}}{\partial y_i}\right|_{\hat{y}} \left.\frac{\partial P_m^{ex}}{\partial y_j}\right|_{\hat{y}} V_{ij}\,, \tag{81}$$

[10] To be more accurate, the electromagnetic coupling should be evaluated for each resonance individually at the corresponding resonance mass. The resulting differences, however, are smaller then the assumed error in $\tilde{\alpha}_{em}$ itself and therefore neglected.

where

$$V_{ij} = \begin{pmatrix} (\delta\Gamma_{1S})^2 & \overline{\delta\Gamma_{1S}\,\delta\Gamma_{2S}} & \cdots & \overline{\delta\Gamma_{1S}\,\delta\Gamma_{6S}} & 0 & 0 \\ \overline{\delta\Gamma_{2S}\,\delta\Gamma_{1S}} & (\delta\Gamma_{2S})^2 & \cdots & \overline{\delta\Gamma_{1S}\,\delta\Gamma_{6S}} & 0 & 0 \\ \vdots & \vdots & \ddots & \vdots & \vdots & \vdots \\ \overline{\delta\Gamma_{6S}\,\delta\Gamma_{1S}} & \overline{\delta\Gamma_{6S}\,\delta\Gamma_{2S}} & \cdots & (\delta\Gamma_{2S})^2 & 0 & 0 \\ 0 & 0 & \cdots & 0 & (\delta\tilde{\alpha}_{em})^2 & 0 \\ 0 & 0 & \cdots & 0 & 0 & (\delta r_c)^2 \end{pmatrix} . \tag{82}$$

The symbol $|_{\hat{y}}$ indicates that the functions are evaluated at the corresponding central values.

The fitting procedure if complicated by the fact that the theoretical uncertainties (coming from the dependence of the theoretical moments on the renormalization scales $\mu_{\rm soft}$, $\mu_{\rm hard}$ and $\mu_{\rm fac}$) are much larger than the experimental errors, which are dominated by the errors in Γ_{1S}, Γ_{2S} and Γ_{3S}. Further, while it is reasonable to assume that the errors in the experimental data can be treated as Gaussian, this is certainly not the case for the "uncertainties" (or better "freedom") in the choices of the renormalization scales for which just a "reasonable" window can be given. It would therefore be inconsistent to include the theoretical uncertainties into the covariance matrix S. Nevertheless, it is important to have some means to combine both types of errors, the experimental and the theoretical ones. In this work this is realized by scanning all scales over the ranges given in Eqs. (17). We will carry out two kind of fits. First, we fit for M_b and α_s simultaneously without taking into account any constraints on α_s, i.e. ignoring all existing determinations of the strong coupling (Section 6.1), and, second, we fit for M_b assuming that α_s is a known parameter i.e. taking into account a constraint on α_s (Section 6.2).

To fit for M_b and α_s simultaneously we employ a strategy closely related to the one suggested by Buras [45] and adopted by the BaBar collaboration [46] as a method to extract Cabibbo-Kobayashi-Maskawa matrix elements from various B-decays. Our strategy consists of the following two steps:

(a) We first choose the range over which the renormalization scales $\mu_{\rm soft}$, $\mu_{\rm hard}$ and $\mu_{\rm fac}$ have to be scanned individually. For convenience we also count the constant r_c, the correlation parameter a_{cor} and the various sets of n's for which the fits shall be carried out as theoretical parameters. The individual ranges employed in this work are as follows,

$$\begin{aligned} 1.5\,\text{GeV} \le\ & \mu_{\rm soft} && \le 3.5\,\text{GeV} \\ 2.5\,\text{GeV} \le\ & \mu_{\rm hard} && \le 10\,\text{GeV} \\ 2.5\,\text{GeV} \le\ & \mu_{\rm fac} && \le 10\,\text{GeV} \\ 0.5 \le\ & r_c && \le 1.5 \\ 0 \le\ & a_{cor} && \le 1\,. \end{aligned} \tag{83}$$

The sets of n's for which we perform the fits are

$$\{n\} = \{4,5,6,7\}\,,\{7,8,9,10\}\,,\{4,6,8,10\}\,. \tag{84}$$

The scanning over the ranges and sets given above is carried out by using a Monte-Carlo generator.

(b) Then, for each set of theoretical parameters

$$\mathcal{M} = \{\mu_{\rm soft}\,, \mu_{\rm hard}\,, \mu_{\rm fac}\,, r_c\,, a_{cor}\,, \{n\}\}\,, \tag{85}$$

called a "model", we construct the χ^2 function as describe before and determine the 95% confidence level (CL) contour in the M_b-α_s-plane by calculating the minimum χ^2, χ^2_{min}, and drawing the contour $\chi^2(M_b, \alpha_s) = \chi^2_{min}+6$. The external envelope of the contours obtained for all models generated by scan represent the "overall 95% CL contour" which we will refer to as the "allowed range for M_b and α_s". It should be mentioned that we do not impose a χ^2 cut which would eliminate models for which the probability of χ_{min} would be smaller than 5%. We will come back to this point in Section 6.

We would like to emphasize that the allowed region for M_b and α_s obtained by the procedure described above should not be understood in any statistical sense. In fact, it is quite difficult to ascribe any accurately defined meaning to the allowed region at all without reference to the method how it has been obtained. This is a consequence of the fact that the theoretical uncertainties, which cannot be apprehended statistically, dominate over the experimental ones.

For the fit for M_b where α_s is assumed to be a known parameter we treat α_s like the theoretical parameters $\mu_{\rm soft}\,, \mu_{\rm hard}\,, \mu_{\rm fac}\,, r_c\,, a_{cor}$ and $\{n\}$, i.e. we also scan over the given range of α_s. The fit for M_b is then carried out in the same way as for the unconstraint fit described before. The only difference is that in this case the 95% confidence level "contour" for each model is determined by the equation $\chi^2(M_b) = \chi^2_{min} + 4$ because this method does represent only a one parameter fit. Some more remarks to this method can be found in Section 6.2.

6 Numerical Results and Discussion

In this section we present the numerical results for the bottom quark pole mass M_b gained from fitting the theoretical moments at NNLO calculated in Section 3 to the experimental moments obtained from experimental data. In Section 6.1 we discuss the result if M_b and α_s are fitted simultaneously ("unconstraint fit") and in Section 6.2 we present the result for M_b if α_s is taken as an input ("constraint fit").

6.1 Determination of M_b and α_s without Constraints

The result for the allowed region for M_b and α_s when both parameters are fitted simultaneously and no previous determination of α_s is taken into account is displayed in Fig. 10. The gray shaded region represents the allowed region in the M_b-α_s plane. To illustrate that the allowed region does not have any well defined statistical meaning we have also shown the dots representing the best fits (i.e. the points in the M_b-α_s plane with the lowest χ^2 value for a large number of models. In fact, the region covered by the dots for the best fits is a measure for the size of the theoretical uncertainties inherent to our result. The latter uncertainties, which cannot be apprehended statistically, clearly dominate over the experimental ones, which are contained in the grey shaded region not covered by any dots. For convenience of the reader we have shown the result for α_s at the scale $\mu = 2.5$ GeV (lower frame axis) and $\mu = M_z$ (upper frame axis) where we have used two-loop running for the strong

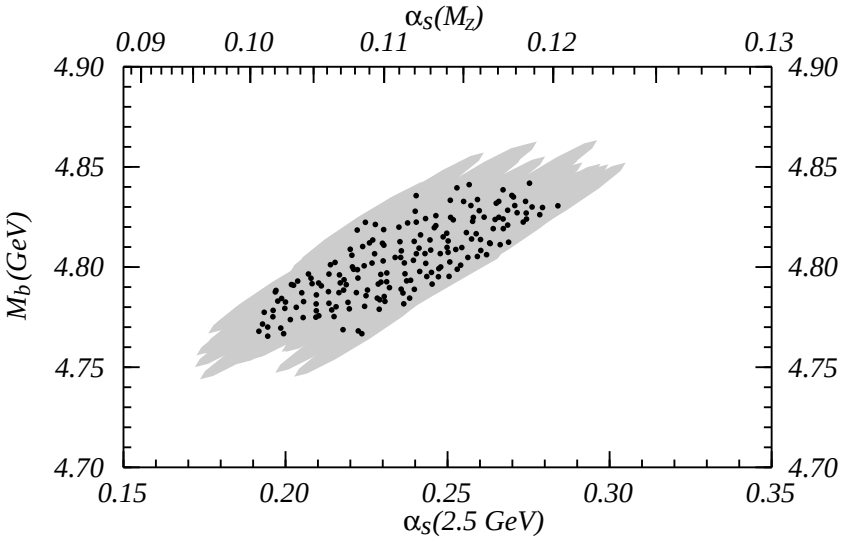

Figure 10: Result for the allowed region in the M_b-α_s plane for the unconstraint fit based on the theoretical moments at NNLO. The grey shaded region represents the allowed region. Experimental errors are included at the 95% CL level. The dots represent point of minimal χ^2 for a large number of models.

coupling. From the shape and orientation of the gray shaded region in Fig. 10 it is evident that M_b and α_s are positively correlated. This can be easily understood from the fact that the theoretical moments are monotonically increasing functions of α_s but monotonically decreasing functions of M_b (see Tab. 2). However, we refrain from presenting a numerical value for the correlation because, as already mentioned, the allowed region for M_b and α_s does not have any statistical meaning.

For the bottom quark pole mass and the strong coupling we obtain

$$4.74 \text{ GeV} \leq M_b \leq 4.87 \text{ GeV}, \tag{86}$$

$$0.096 \leq \alpha_s(M_z) \leq 0.124, \tag{87}$$

$$0.175 \leq \alpha_s(2.5 \text{ GeV}) \leq 0.308. \tag{88}$$

(NNLO analysis, M_b and α_s are fitted simultaneously)

Because the uncertainties for M_b and α_s are not Gaussian we only present the allowed ranges obtained from Fig. 10. We would like to emphasize that in this context the inequality sign "$\leq$" does not have any mathematical meaning. It is only used to describe the bounds on M_b and α_s which are obtained from our fitting procedure. The allowed range for M_b, which spans over 120 MeV, can be definitely called a precise determination of the bottom quark pole mass. The allowed range obtained for the strong coupling, on the other hand, is consistent with the current world average, but much wider than the uncertainties of the latter. In addition, most of the allowed range for α_s is located below the current world average. Taking the size of allowed ranges for M_b and α_s as their uncertainty we arrive

at

$$\frac{\Delta M_b}{M_b} \sim 2.5\ \%\,, \tag{89}$$

$$\frac{\Delta \alpha_s(M_z)}{\alpha_s(M_z)} \sim 25\ \%\,, \tag{90}$$

$$\frac{\Delta \alpha_s(2.5\ \mathrm{GeV})}{\alpha_s(2.5\ \mathrm{GeV})} \sim 50\ \%\,, \tag{91}$$

for the relative uncertainties in our determination of M_b and α_s. It is evident that the sum rule based on the large n moments, Eq. (3), is much more sensitive to the bottom quark mass than to the strong coupling. At least at the present stage one can certainly conclude that this sum rule does not belong to most powerful methods to determine α_s as far as precision is concerned.

From Eqs. (86) and (87) we can calculate the value for the running bottom quark mass. Using the two-loop relation between the pole and running mass [47] (see also Ref. [41] and references therein) and taking into account the correlation between the pole mass and the strong coupling we get

$$4.09\ \mathrm{GeV} \leq m_b(M_{\Upsilon(1S)}/2) \leq 4.32\ \mathrm{GeV}\,, \tag{92}$$

$$4.17\ \mathrm{GeV} \leq m_b(m_b) \leq 4.35\ \mathrm{GeV}\,. \tag{93}$$

This result is in excellent agreement with a recent determination of the running bottom quark mass obtained from the three-jet rate in $b\bar{b}$ events at the CERN e^+e^- LEP experiment DELPHI [49, 48], $m_b(M_{\Upsilon(1S)}/2) = 4.16 \pm 0.14$ GeV. The uncertainty in the result for the running quark mass, Eq. (93), is larger than for our pole mass result, Eq. (86), because of the correlation between M_b and α_s, which has to be taken into account in the conversion formula.

We have checked that the allowed region for M_b and α_s presented in Fig. 10 is insensitive to the particular choices of the scanning ranges for the renormalization scale $\mu_{\rm hard}$ and the constants a_{cor} and r_c, which parameterize the correlation of the experimental data for the electronic widths and the continuum cross section above the $B\bar{B}$ threshold, respectively. However, the results depend on the choice of the ranges for the soft scale $\mu_{\rm soft}$ and the factorization scale $\mu_{\rm fac}$. This dependence is illustrated in Fig. 11 where we have displayed points for the best fits (a) for models with $1.5\,\mathrm{GeV} \leq \mu_{\rm soft} \leq 2.5\,\mathrm{GeV}$ and $2.5\,\mathrm{GeV} \leq \mu_{\rm soft} \leq 3.5\,\mathrm{GeV}$ and (b) for models with $2.5\,\mathrm{GeV} \leq \mu_{\rm fac} \leq 5.0\,\mathrm{GeV}$ and $5.0\,\mathrm{GeV} \leq \mu_{\rm soft} \leq 10\,\mathrm{GeV}$ with different symbols. In both figures the other parameters have been scanned over the ranges given in Eqs. (83). From Fig. 11(a) we see that the allowed range for M_b does not depend significantly on the choice for the soft scale, whereas the allowed range for α_s tends toward larger values if the soft scale is larger. Fig. 11(b), on the other hand, shows that the size of the allowed range for M_b could be reduced if smaller factorization scales would be chosen. In that case the allowed range for α_s would be only mildly affected. From this observation it might be tempting to choose the scanning range for $\mu_{\rm soft}$ at higher scales and for $\mu_{\rm fac}$ at lower scales because this would lead to a seemingly more precise determination of M_b and higher values for α_s. However, we take the position that the choice of the scanning ranges for the renormalization scales should not depend on such considerations to represent a "reasonable choice". In fact, we consider it inappropriate to tune or "optimize" renormalization scales in some specific way if no good physical reason for that can be given. In our case the choice for the scanning ranges for the soft scale was motivated by the fact that it governs the nonrelativistic correlators for which (at NNLO) the relative momentum of the

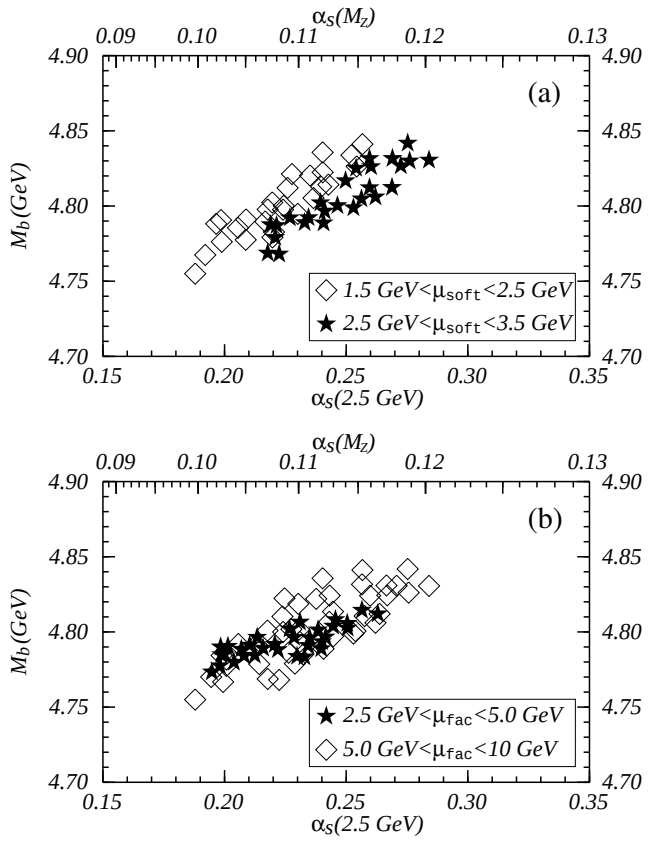

Figure 11: Typical distribution of points representing the best fits (a) for models with $1.5\,\text{GeV} \leq \mu_{\text{soft}} \leq 2.5\,\text{GeV}$ and $2.5\,\text{GeV} \leq \mu_{\text{soft}} \leq 3.5\,\text{GeV}$ and (b) for models with $2.5\,\text{GeV} \leq \mu_{\text{fac}} \leq 5.0\,\text{GeV}$ and $5.0\,\text{GeV} \leq \mu_{\text{soft}} \leq 10\,\text{GeV}$ based on the theoretical moments at NNLO. The other parameters are scanned over the ranges given in Eqs. (83).

bottom quarks (which is of order $M_b\alpha_s$) represents the only relevant physical scale. Our choice for factorization scale μ_{fac}, on the other hand, is inspired by the belief that is can take any value between the relative momentum of the bottom quarks and the hard scale which is of order the bottom quark mass (see Section 2). We will come back to this issue in Section 7.

It is very interesting to compare the results of our NNLO analysis presented above to an analogous analysis based on the NLO moments, i.e. ignoring all the NNLO contributions. [See the end of Section 3 for a prescription how the NLO moments can be recovered from the NNLO ones.] The result for the allowed range for M_b and α_s based on the NLO moments is displayed in Fig. 12. The gray shaded region and the dots have been obtained in the exactly the same way as described for the NNLO analysis. For comparison we have also indicated the allowed region obtained from the NNLO analysis by a polygon. Evidently the allowed region for M_b and α_s covers a much larger area for the NLO analysis than for the NNLO one. At NLO the result for bottom quark pole mass and the strong coupling read

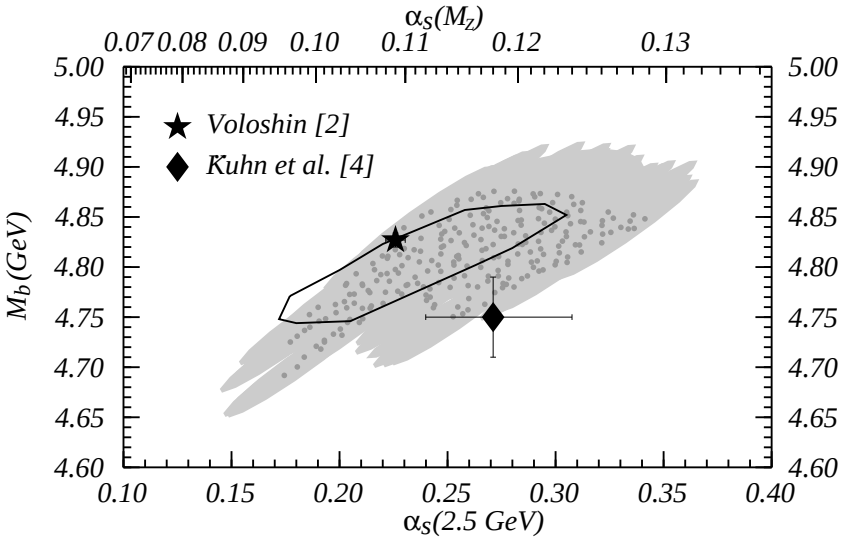

Figure 12: Result for the allowed region in the M_b-α_s plane for the unconstraint fit based on the theoretical moments at NLO. The grey shaded region represents the allowed region. Experimental errors are included at the 95% CL level. The dots represent point of minimal χ^2 for a large number of models. The star and the diamond represent the results obtained by Voloshin [2] and Kühn *et al.* [4], respectively. The error-bars quoted by Voloshin are smaller than the symbol used to display his central value. The polygon represents the allowed region obtained from the NNLO analysis.

$$4.64 \text{ GeV} \leq M_b \leq 4.92 \text{ GeV}, \tag{94}$$

$$0.086 \leq \alpha_s(M_z) \leq 0.132, \tag{95}$$

$$0.144 \leq \alpha_s(2.5 \text{ GeV}) \leq 0.368. \tag{96}$$

(NLO analysis, M_b and α_s are fitted simultaneously)

From Fig, 12 and Eqs. (94) – (96) it is evident that the inclusion of the NNLO contributions of the moments leads to a considerable improvement upon a pure NLO analysis. We would like to point out that the uncertainties in M_b and α_s from our NLO analysis are much larger then the uncertainties quoted by Voloshin [2] and Kühn *et al.* [4]. For comparison we have also displayed the results from Refs. [2, 4] in Fig. 12. Because the theoretical moments used in Refs. [2, 4] and the NLO moments used to generate the allowed region for M_b and α_s displayed in Fig. 12 are equivalent, we consider the small uncertainties quoted in Refs. [2, 4] as a consequence of an inappropriate treatments of the large theoretical uncertainties inherent to the perturbative calculations of the moments. (See Section 7 for a more detailed discussion.) Another way to see that that the NNLO contributions lead to a considerable improvement is to compare the distributions of best χ^2 values which are achieved by the models based on NNLO and NLO moments, respectively. In Tab. 7 the fraction (in percent) of best χ^2 values within certain intervals is displayed for the NNLO and the NLO analysis based on,

χ^2_{min}	$0-3$	$3-6$	$6-10$	$10-15$	$15-20$	$20-30$	$30-50$	$50-100$	$100-\infty$
NNLO	28 %	17 %	16 %	22 %	8 %	4 %	2 %	3 %	0 %
NLO	0 %	0 %	0 %	0 %	0 %	1 %	7 %	35 %	57 %

Table 7: Distributions of best χ^2 values for a NNLO and NLO analysis based on, at each case, 1300 randomly generated models within the ranges (83).

at each case, 1300 randomly generated models within the scanning ranges in Eqs. 83. Whereas for the NNLO analysis more than 60 % of the models have a best χ^2 value below 10, the bulk of the best χ^2 values for the NLO analysis is larger than 50. We would like to emphasize that, because the uncertainties of the analysis are dominated by theory, the distributions of best χ^2 values in Tab. 7 represent only a measure for the quality of the theoretical expression for the moments, but do not contain any statistical information. We therefore cannot impose a χ^2 on the models, let us say, based on an assumed statistical distribution of χ^2 values. As an example, for two degrees of freedom and at the 95 % CL, and assuming a Gaussian distribution such a χ^2 cut would eliminate all models whose best χ^2 value is larger than 6. Evidently, in this case, none of the models based on the NLO moments would survive and we would be forced to reject, at least, the nonrelativistic expansion up to NLO as a legitimate tool to calculate the moments from QCD for the sets of n's considered in this work.

6.2 Determination of M_b with Constraints on α_s

We now carry out the fitting procedure for M_b if α_s is taken as an input, e.g. from the current world average. At this point one might be tempted to simply cut out of the gray shaded region in Fig. 10 the part for which α_s is located in the preferred range. Due to the sizable correlation between M_b and α_s this would then lead to a much smaller uncertainty in M_b than given in Eq. (86). However, the naive procedure just described is not the correct way to account for a constraint on α_s. This comes from the fact that for the unconstraint fit performed in Section 6.1 the strong coupling is essentially a function of the model parameters $\mathcal{M} = \{\mu_{\rm soft}, \mu_{\rm hard}, \mu_{\rm fac}, r_c, a_{cor}, \{n\}\}$, i.e. α_s is not independent of the choice for $\mathcal{M}$. If α_s is taken as an input, however, we have to treat α_s and $\mathcal{M}$ as independent, because we have to be able to freely assign values to them. Thus, if we take α_s from the world average, we can expect that for a number of models the allowed range for M_b will be located outside the gray shaded region in Fig. 10. As a consequence, the constraint fit will in general lead to larger uncertainties in M_b than the unconstraint one. In addition, due to the positive correlation between M_b and α_s we can also expect that the result for the allowed region of M_b for the constraint fit will be located at slightly larger masses than for the unconstraint fit.

We would like to point out that there are many ways to account for a constraint on α_s which all might lead to slightly different results. In this work we account for a constraint on α_s by treating it in the same way as the parameters in $\mathcal{M}$, i.e. we also scan over the preferred range of α_s. The allowed range of M_b is then obtained in the same way as for the unconstraint fit carried out in Section 6.1 with the difference that now only a one-parameter fit is performed (see also Section 5). It should be noted that this method treats α_s entirely on the same footing as the theoretical parameters in $\mathcal{M}$,

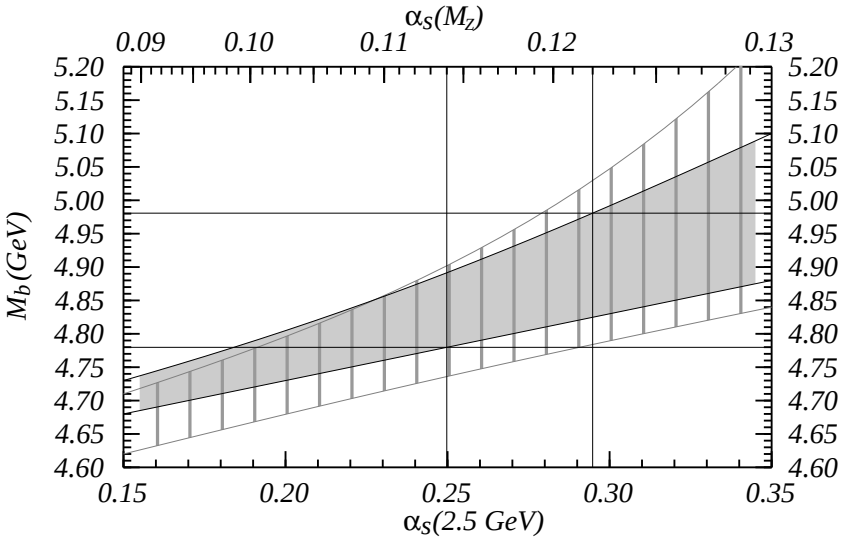

Figure 13: Result for the allowed M_b values for a given value of α_s. The grey shaded region corresponds to the allowed ranges for the NNLO analysis and the striped region for the NLO analysis. Experimental errors are included at the 95% CL level. It is illustrated how allowed range for M_b at NNLO is obtained if $0.114 \leq \alpha_s(M_z) \leq 0.122$ is taken as an input.

i.e. the uncertainties on α_s are not taken into account as Gaussian or statistical errors. In Fig. 13 the allowed range for M_b based on the NNLO moments is presented as a function of α_s. For each given value for α_s the allowed range for M_b, which is obtained by scanning all the parameters in $\mathcal{M}$ over the ranges (83), is the projection of the gray shaded region onto the M_b axis. If a region for α_s is given the allowed range for M_b is obtained by projecting the gray shaded region for all the α_s valued in the preferred region onto the M_b axis. As an example which is also illustrated in Fig. 13, staring from the world average for α_s as given by Stirling [1], $0.114 \leq \alpha_s(M_z) \leq 0.122$, we arrive at

$$4.78 \text{ GeV} \quad \leq \quad M_b \quad \leq \quad 4.98 \text{ GeV} \tag{97}$$

(NNLO analysis, $\alpha_s(M_z)$ taken from the world average [1])

for the bottom quark pole mass. The result is consistent with Eq. (86) obtained from the unconstraint fit. However, as expected, the allowed range for M_b is wider and, in addition, located at slightly larger masses. In fact, the uncertainty on M_b for the constraint for is almost a factor of two larger. We have checked that the result for M_b is insensitive to the particular choice of the scanning ranges for $\mu_{\rm hard}$, $\mu_{\rm fac}$, a_{cor} and r_c. However, the bottom quark mass tends toward lower values if $\mu_{\rm soft}$ is chosen larger. We have also displayed the result for the NLO analysis in Fig. 13 as the striped area. As for the unconstraint fit the inclusion of the NNLO contributions to the moments leads to a smaller uncertainty for M_b, although the improvement is not as dramatic. We want to mention that the larger uncertainty for M_b obtained from the constraint fit is partly a consequence of the fact that our fitting procedure does not treat the error on α_s as Gaussian or statistical. Therefore one might argue that the

uncertainties in Eq. (97) are too conservative. However, from the way how a world average is gained, it is certain that the error of α_s constrains a sizable systematic contribution. Because an accurate quantitative description of such a systematic error is quite difficult, we take the position that the error on α_s should be treated in a conservative way.

Using the result in Eq. (97) and the two-loop relation between the running and the pole mass [47] we obtain

$$4.08\ \text{GeV} \quad \leq \quad m_b(M_{\Upsilon(1S)}/2) \quad \leq \quad 4.28\ \text{GeV}\,, \tag{98}$$

$$4.16\ \text{GeV} \quad \leq \quad m_b(m_b) \quad \leq \quad 4.33\ \text{GeV}\,. \tag{99}$$

for the running bottom quark mass. It is remarkable that this result and the result for the running quark mass based on the unconstraint fit, Eq. (93), are almost identical.

7 Comments on Previous Analyses

In the past few years there have been three previous analyses by Voloshin [2], Jamin and Pich [3] and Kühn, Penin and Pivovarov [4] where the bottom quark pole mass and the strong coupling have been extracted from data on the Υ mesons and using the same sum rule as in our analysis. We would like to emphasize that in Refs. [2, 3, 4] no consistent determination of NNLO corrections has been carried out and that the results by Voloshin

$$M_b = 4.827 \pm 0.007\ \text{GeV}\,, \qquad \alpha_s(M_z) \,=\, 0.109 \pm 0.001\,, \qquad \text{(Voloshin)} \tag{100}$$

Jamin and Pich (JP)

$$M_b = 4.60 \pm 0.02\ \text{GeV}\,, \qquad \alpha_s(M_z) \,=\, 0.119 \pm 0.008\,, \qquad \text{(Jamin, Pich)} \tag{101}$$

and Kühn, Penin and Pivovarov (KPP)

$$M_b = 4.75 \pm 0.04\ \text{GeV} \qquad \alpha_s(M_z) \,=\, 0.118 \pm 0.006\,, \qquad \text{(Kühn } \textit{et al.}\text{)} \tag{102}$$

are contradictory to each other and partly to our own results. In particular, although no NNLO contributions have been included, all results in Refs. [2, 3, 4] are claimed to have much smaller uncertainties than any of the results obtained in our analyses. In this section we will explain the origin of those discrepancies and give some comments on the methods used in Refs. [2, 3, 4] from the point of view of the strategies followed in this work. To organize the discussion we will analyze the methods used in Refs. [2, 3, 4] with respect to three aspects: (i) theoretical expression for the moments, (ii) optimization and tuning of the perturbative series for the moments and (iii) fitting procedure and error analysis. Because the theoretical uncertainties in the determination of M_b and α_s are much larger than the experimental ones, we will neither focus on the treatment of experimental errors nor on the formulae used for the experimental moments. Compared to the effects caused by using different methods to handle the theoretical uncertainties, the differences in the treatment of the experimental side of the analysis represent only a minor issue. We also would like to mention that in the analyses of Voloshin, JP and KPP moments with n as large as 20 were used. According to the estimates given in Section 2 this means that the effective smearing range contained in those moments is already of the

same size as or even smaller than $\Lambda_{\rm QCD}$. This leads to a an additional source of systematic theoretical errors in the results of Voloshin, JP and KPP. We have checked, however, that using moments with $10 \leq n \leq 20$ causes only shifts in the results for M_b (and α_s) which are small compared to the size of the theoretical uncertainties at the NLO level as we have estimated them in our analysis. Therefore we will not raise this issue in the following discussion. For a NNLO analysis, however, where the uncertainties in M_b are shown to be smaller, the use of values of n which are too large is an important issue and can lead to considerable errors.

Theoretical expressions for the moments:

Voloshin's moments are identical to ours at the NLO level.

The moments used by KPP have been calculated in the same way as Voloshin's (and ours at the NLO level) with the difference that the dispersion relation in Eq. (4) has been performed numerically in terms of it covariant form, i.e. without using the asymptotic expansion (47) and the inverse Laplace transform. We have checked that for the values of n's considered by Voloshin, KPP and us the difference between both approaches is negligible. Thus, the moments used by KPP are equivalent to Voloshin's and ours at the NLO level.

The moments by JP, on the other hand, were obtained from the Born, one-loop and two-loop expressions for $R(e^+e^- \to b\bar{b})$ supplemented by a resummation of LO Coulomb singularities in form of the Sommerfeld factor (see Eq. (32)). Further, the one-loop corrections to the Coulomb potential have been implemented by inserting them directly into the Sommerfeld factor, i.e. without using time-independent perturbation theory. For the dispersion integration (4) JP have only taken into account c.m. energies above the threshold point ($s > 4M_b^2$). We disagree with the moments used by JP in two major points. Most important, JP did not take into account the bound state poles of the cross section R, which are located below the threshold point ($s < 4M_b^2$). We have demonstrated in Section 4 that the bound states represent the dominant contribution to the moments for large values of n (see Tab. 4). Thus the moments used by JP are far too small which causes the bottom quark pole mass obtained from the fits to be too low.[11] In fact, one can easily see that omitting the bound state poles for large values of n will always lead to a bottom quark pole mass $M_b \leq M_{\Upsilon(1S)}/2 \approx 4.7$ GeV regardless whether α_s is determined from the fit or taken as an input. This explains why the value for M_b in the analysis by JP is significantly smaller than in the analyses by Voloshin, KPP and us. In addition, we do not think that the effects of the running of the Coupling governing the Coulomb potential have been treated properly. JP simply inserted the one-loop corrections to the Coulomb potential into the Sommerfeld factor. Whereas this legitimate for the non-logarithmic corrections, it is not for the logarithmic ones because the effects arising from virtual momenta below and above the scale $\sim M_b\alpha_s$ are not taken into account correctly. This can only be achieved by using time-independent perturbation theory (or by solving the Schrödinger equation exactly). We therefore conclude that the results obtained by JP contain large systematic theoretical errors which are by far larger than indicated by their error analysis. That the value for α_s obtained by JP still seems reasonable is a consequence of the fact that the moments are much less sensitive to α_s than to M_b.

Optimization and Tuning:

[11] The same conclusion has been drawn in Ref. [4].

We have shown in Section 4 that the perturbative corrections to the moments and the resulting scale dependences are quite large. This behavior is particularly obvious at the NNLO level. However, already at NLO the corrections are uncomfortably large. In our analysis this feature has been fully taken into account during our fitting procedure. In fact, it is the main source of theoretical uncertainties in our results. In the analyses by Voloshin and KPP, however, the perturbative expansion for the theoretical moments has been tuned to improve the convergence.

In Voloshin's work, at each value of n the soft scale $\mu_{\rm soft}$ has been fixed such that the NLO corrections caused by $V_c^{(1)}$, Eq. (19), vanish exactly and the hard scale $\mu_{\rm hard}$ has been fixed to the BLM scale [50]. Thus, Voloshin has eliminated the scale dependences of the moments. We would like to emphasize that we consider Voloshin's prescription as one possible choice for the renormalization scales, which essentially corresponds to selecting one single model out of the range of models used in our analysis. We have shown in Section 6 (see e.g. Fig. 10) that the results for M_b and α_s depend significantly on such a choice. Because we think that no argument can be found why Voloshin's choice should be better than others, we have the position that a scan over all "reasonable" models should be carried out. Because Voloshin has not carried out such a scan we consider the theoretical uncertainties quoted in his analysis as largely underestimated.

In the analysis by KPP, at each value of n a non-logarithmic piece of $V_c^{(1)}$ has been absorbed into the LO nonrelativistic Green function, Eq. (31), such that the NLO corrections caused by the non-absorbed piece (calculated via first order time-independent perturbation theory) vanish. This optimization is quite similar to Voloshin's but leaves the soft scale unfixed. It should be mentioned that KPP have explicitly identified soft and hard scale which has eliminated the possibility to vary both scales independently. This reveals why the uncertainties quoted by KPP are much larger than Voloshin's, and partly explains why they are still much smaller than the uncertainties obtained from our NLO analysis where no optimization has been performed. (See Fig. 12 for a graphical comparison).

JP have not carried out any optimization. However, due to their way to calculate the moments starting from the expressions of the covariant multi-loop expressions for the cross section, JP implicitly identified soft and hard scale.

Fitting procedure and error estimate:

In the analysis by Voloshin and KPP a two parameter fit was carried out to obtain M_b and α_s for the sets $\{n\} = \{8, 12, 16, 20\}$ and $\{10, 12, 14, 16, 18, 20\}$, respectively. Thus, the results obtained by Voloshin and KPP should be compared with the results of our unconstraint fit presented in Section 6.1. Because Voloshin has eliminated all scale dependences, he has estimated the theoretical uncertainties in his analysis using the assumption that the NNLO corrections to the n'the moments can be parameterized by a global factor $(1 + c/n)$ where c is a number of order one. The size of the uncertainties was obtained from the variation of the best fits for M_b and α_s if c is first fixed to zero and then obtained from a three parameter fit. The theoretical uncertainties gained by this method have been of the same size as the (small) experimental errors. We have shown in Section 4 that the NNLO contributions to the moments have an entirely different structure (large size, growing with n, tremendous dependence on the soft scale) and cannot be accounted for by the global factor $(1+c/n)$. Thus, Voloshin's method to estimate the theoretical error is not capable to account for the true size of theoretical uncertainties inherent to the perturbative calculation of the moments.

In the analysis by JP the theoretical uncertainties for M_b and α_s were essentially obtained from the variation of the best fit for M_b and α_s (for fixed $\mu_{\rm soft} = \mu_{\rm hard} = M_b$) when the two-loop corrections to the Coulomb potential, $V_c^{(2)}$, are included and when the two-loop contributions to the high energy cross section are removed. No additional uncertainties (e.g. from the renormalization scale dependence) have been taken into account based on the argument that this would lead to a double counting of theoretical uncertainties. We disagree with this statement because the effects of the inclusion or removal of the two-loop corrections to the high energy cross section or the Coulomb potential certainly depends on the value of the other parameters (like the renormalization scales). This and the fact that JP have neglected the bound state poles, which are the dominant source of large corrections to the moments (and their scale dependence) for large values of n, have lead to an underestimate of the theoretical uncertainties (besides the large systematic errors mentioned above).

KPP, finally, have determined M_b and α_s separately. For the determination of M_b $\alpha_s(M_z) = 0.118$ was taken as a fixed input. Thus, the result for M_b by KPP should be compared to the results of our constraint fit presented in Section 6.2. The method used by KPP to obtain M_b was based on solving the equation $P_n^{th} = P_n^{ex}$ for M_b while n and all the other parameters are fixed to specific values. The mean value and the uncertainty for M_b has then been gained by calculating the mean and observing the spread of M_b values when this procedure was carried out, first, for $\mu_{\rm soft} = \mu_{\rm hard} = M_b$ and $n = 10, 12, \ldots, 20$ and, second, for fixed $n = 14$ and $1.2\,{\rm GeV} \leq \mu_{\rm soft} = \mu_{\rm hard} \leq M_b$. This procedure effectively scans over some fraction of the range of models used in our fitting procedure but misses e.g. models with $n \neq 14$ and $\mu_{\rm soft} \leq M_b$. This the main reason why the uncertainties quoted by KPP are much smaller than in our NLO analysis.

From the discussion presented above we come to the following final conclusion about the results by Voloshin, JP and KPP in comparison to our own analysis: The theoretical moments calculated by Voloshin and KPP are equivalent to our NLO moments. We therefore consider the results obtained by Voloshin and KPP consistent with our own results at the NLO level (see Fig. 12 and 13). However, the theoretical uncertainties are underestimated in both analyses, which leads to the apparent contradiction between the results by Voloshin and KPP. In view of the error analysis performed in our analysis, where we tried to impose as less bias as possible, the results by Voloshin and KPP are perfectly consistent. The apparent contradiction essentially corresponds to a disjunct (and from our point of view biased) choice of models used for the fitting procedure in both analyses. We want to emphasize that the choice by Voloshin is not less plausible than the one made by KPP which illustrates the need that the whole range of models must be scanned in the fitting procedure. The comparison between the results of our analysis, where such a complete scan has been performed, and the results obtained by Voloshin and KPP makes this obvious. The theoretical moments determined by JP, on the other hand, do not take into account the bound state poles which represent the dominant contributions to the moments for large values of n. As a consequence the M_b value obtained by JP is too small and has to be considered inconsistent with the results by Voloshin, KPP and us and, in particular, with the nonrelativistic expansion of QCD, where the bound state poles are predicted. That the value for α_s obtained by JP still seems reasonable is a consequence of the fact that the moments are much less sensitive to α_s than to M_b.

While this paper was in its final stages there appeared a letter by Penin and Pivovarov (PP) [51] where the NNLO corrections to the large n moments have also been included in the sum rule deter-

mination of the bottom quark pole mass. The formulae for the moments used by PP were based on previous results for the cross section published in [7, 8, 9, 10] and are therefore conceptually equivalent to ours. For the bottom quark pole mass PP quote the result $M_b = 4.78 \pm 0.04$ GeV. The result is consistent with ours. The uncertainty, however, is smaller and the allowed range for M_b is somewhat lower than for our NNLO results. To obtain this apparently more precise result PP have used the same methods as in Ref. [4] (which we have already criticized above) with the difference that all the scales (including the factorization scale) were varied in the range $M_b \pm 1$ GeV. We consider this range too high for the soft scale. Further, there is a sign error in the $C_A C_F$ piece of the $\mathcal{O}(\alpha_s^2)$ short-distance coefficient in Eq. (2) of [51], which is not contained in the original publication [9], and in Eqs. (43) and (45) of this paper. These issues and the fact the PP used values of n for the moments between 10 and 20, which we consider too large for a NNLO analysis, are the main reasons why the result by PP is located at lower masses. Further, we would like to point out two mistakes in [51] which, however, do not affect the results for M_b. PP state that the knowledge of the nonrelativistic correlators is sufficient to completely determine the vacuum polarization function, Eq. (1), in the threshold regime. This is not true due to UV-divergences in the real parts of the correlators which still have to be removed by an additional matching calculation. (See the discussion at the end of Section 3.2.) PP state that the factorization scale $\mu_{\rm fac}$ in the $\mathcal{O}(\alpha_s^2)$ short-distance constant and in the correlators (Eqs. (2), (5) and (6) in [51])) is defined in the $\overline{\rm MS}$ scheme. This statement is not true. The formulae used by PP were taken from Ref. [9] where the factorization scale is defined in a cutoff scheme. The corresponding results in the $\overline{\rm MS}$ scheme can be obtained by an additional redefinition of the factorization scale $\mu_{\rm fac}$. (See the discussion following Eq. (31).)

8 Conclusions and Outlook

Based on the argument of global duality and causality one can relate the derivatives of the vacuum correlator of two bottom-antibottom vector currents at zero momentum transfer to an integral over the total cross section of the production of hadrons containing a bottom and an antibottom quark in electron-positron annihilation

$$P_n \equiv \frac{4\,\pi^2\,Q_b^2}{n!\,q^2}\left(\frac{d}{dq^2}\right)^n \Pi_\mu{}^\mu(q)\Big|_{q^2=0} = \int \frac{ds}{s^{n+1}}\,R^{b\bar{b}}(s)\,, \tag{103}$$

It is therefore possible to relate a theoretical calculation of the moments P_n to experimental data for the cross section $R(e^+e^- \to$ "$b\bar{b}$ hadrons"). The limit of large values of n is of special interest for relation (103) because in this limit the high energy contributions are suppressed. For the theoretical side this means that the bottom-antibottom pair can be treated nonrelativistically, and for the experimental side that data for the production of Υ mesons are already sufficient to saturate relation (103). The requirement that the effective range of integration is larger than $\Lambda_{\rm QCD}$ [14] imposes an upper bound on the values of n for which a perturbative calculation of the moments can be trusted. Due to the large size of the bottom quark mass of order five GeV we are in the fortunate situation that a range of values of n can be found for which the $b\bar{b}$ system can be treated nonrelativistically and, at the same time, the range of integration is still broad enough compared to $\Lambda_{\rm QCD}$. We have identified this range of "large values of n" as $4 \lesssim n \lesssim 10$. In this work we have used the arguments just given

to determine the bottom quark pole mass M_b and the strong coupling α_s in the $\overline{\rm MS}$ scheme from experimental data on the Υ masses and electronic decay widths.

The aim of this paper was twofold:

1.) **Calculation of NNLO corrections:** The complete set of NNLO corrections in relation (103) for large values of n has been calculated. This includes corrections to the expressions in the nonrelativistic limit or order α_s^2, $\alpha_s\, v$ and v^2, where v is the velocity of the bottom quarks in the c.m. frame. The conceptual difficulty in those calculations is that the relativistic corrections, e.g. from the kinetic energy or from higher order interactions like the Darwin or the Breit-Fermi potential lead to ultra-violet divergent integrations. We have used the concept of effective field theories formulated in NRQCD [11, 12] to deal with this problem. In NRQCD the latter divergences appear as a natural consequence of the existence of higher dimensional operators which lead to the renormalization of lower dimensional ones. The exact form of the renormalization constants is obtained through matching to full QCD. This automatically provides a separation of all relevant effects into short-distance (contained in the renormalization constants) and long-distance ones (contained in matrix elements). In our case this leads to an expression for the moments (and the cross section $R(e^+e^- \to$ "$b\bar{b}$ hadrons") which is a sum of terms each of which consists of a nonrelativistic current correlator multiplied with a short-distance factor (see Eqs. (13) and (50)). For the leading term in this series we have performed matching at the two-loop level. Although the NNLO contributions are quite large, they lead to a considerable reduction of the theoretical uncertainties in the extraction of M_b.

2.) **Conservative approach for the error estimates:** The uncertainties in the determination of M_b (and α_s) based on sum rule (103) are dominated by theory, in particular, by the remaining large renormalization scale dependences of the theoretical moments. These scale dependences are caused by large coefficients which arise in the perturbative calculation of the corrections to the moments in the nonrelativistic regime. In contrast to statistical errors, which can be treated in a standardized way, it is not an easy task to properly account for theoretical uncertainties, in particular, if a model-independent (in the framework of QCD) analysis is intended. In fact, in an analysis where theoretical uncertainties dominate results may easily become biased depending on personal preferences. For the case of the determination of M_b from sum rule (103) this has lead to the paradoxical situation that in two earlier publications [2, 4] contradictory results were obtained although equivalent theoretical expressions for the moments were used. In this paper it was attempted to include as less personal preference into the analysis as possible by scanning all theoretical parameters independently over *reasonably large* ranges which were in size and location motivated from *general* considerations. For each set of parameters, called a "model", a standard statistical fitting procedure was carried out using the method of least squares to calculate a 95% CL contour. The external envelope of the contours obtained for all the scanned models was then taken as the "overall allowed range" which, we want to emphasize, does not have any well defined statistical meaning due to the dominance of theoretical uncertainties. This makes the scanning method more conservative (and in our opinion also more honest) than the methods used in Refs. [2, 4]. In addition, the scanning method has the advantage that it automatically accounts for non-linear dependences on the theoretical parameters and prevents by construction the Gaussian-like treatment of theoretical uncertainties. Of course, the results presented in this work are not completely free from personal preferences either because of the choice of the ranges used for the scanning.

In this paper we have performed two different analyses based on the scanning method and including the new NNLO corrections. First, M_b and α_s were determined simultaneously using the least squares method for two parameters. We have obtained

$$4.74\ \text{GeV} \leq M_b \leq 4.87\ \text{GeV}\,, \tag{104}$$

$$4.09\ \text{GeV} \leq m_b(M_{\Upsilon(1S)}/2) \leq 4.32\ \text{GeV}\,, \tag{105}$$

$$0.096 \leq \alpha_s(M_z) \leq 0.124 \tag{106}$$

(NNLO analysis, M_b and α_s are fitted simultaneously).

The corresponding result using the NLO expressions for the moments yielded considerably larger uncertainties (see Figs. 10 and 12 and Eqs. (86)–(88) and (94)–(96)). The results show that relation (103) allows for a much more precise determination of the bottom quark mass than for the strong coupling. Second, M_b was determined using the least squares method for one parameter and taking α_s as a known parameter. We have obtained

$$4.78\ \text{GeV} \leq M_b \leq 4.98\ \text{GeV}\,, \tag{107}$$

$$4.08\ \text{GeV} \leq m_b(M_{\Upsilon(1S)}/2) \leq 4.28\ \text{GeV} \tag{108}$$

(NNLO analysis, $0.114 \leq \alpha_s(M_z) \leq 0.122$).

As for the first analysis the NNLO contributions to the theoretical moments lead to a reduction of the uncertainties (see Fig. 13). In our opinion, the sum rule (103) can be regarded as a quite precise tool to determine the bottom quark mass. For the determination of the strong coupling we are by far less optimistic.

In the past few years there have been three previous analyses by Voloshin [2], Jamin and Pich [3] and Kühn *et al.* [4] where the bottom quark pole mass has been determined from experimental data for the masses and the electronic decay widths for the Υ mesons using the sum rule (103). The results obtained in those three analyses are contradictory to each other, and, although NNLO corrections have essentially not been included, quote uncertainties smaller than in our own NNLO analysis. The results obtained by Voloshin and Kühn *et al.* are based on moments which are equivalent to ours at the NLO level. In view of the uncertainties for M_b (and α_s) obtained from our analysis at NLO, the results by Voloshin and Kühn *et al.* can therefore be regarded as consistent with each other (and us), see Fig. 12. The small uncertainties quoted by Voloshin and Kühn *et al.* come from too tight, model-like bounds imposed on the theoretical parameters. The results obtained by Jamin and Pich, on the other hand, contain a large systematic error due to the negligence of the bound state contributions in the moments. We consider the result by Jamin and Pich inconsistent with those by Voloshin, Kühn *et al.* and us, and in particular with the nonrelativistic expansion of QCD.

It is quite interesting to ask whether and how the results determined in this work can be further improved in order to arrive at even smaller uncertainties for the bottom quark pole mass or the strong coupling. From the technical point of view the answer would simply by to calculate the NNNLO contributions in relation (103). Such a task, however, is highly nontrivial. Apart from the fact that a three-loop matching would have to be performed also the NNNLO effects in the bottom-antibottom interactions would have to considered. This would require a consistent treatment of retardation effects which are caused by the non-instantaneous exchange of gluons and, as a prerequisite, a better understanding of higher order Fock bottom-antibottom-gluon states. In principle a calculation to determine these effects would be the QCD analogue of the determination of the Lamb shift contributions to the positronium wave function. So far no technical instruments have been developed yet

to immediately tackle this challenging problem. We further believe that it is unlikely that this goal can be achieved entirely in the framework of perturbation theory because it involves also the bound state energy $\sim M_b\, v^2 \sim M_b\, \alpha_s^2$ as a relevant scale. For the bottom quark this scale is already of the same size as the typical hadronization scale $\Lambda_{\rm QCD}$, which means that the bottom-antibottom-gluon propagation is certainly nonperturbative. In fact, the rather uncomfortably large NNLO corrections in relation (103) might be regarded as a first warning sign in support of this view.

At this point it seems to be just natural to mention the renormalon ambiguities contained in the definition of the pole mass [52] which is defined perturbatively as the location of the singularity of the renormalized quark propagator. This ambiguity indicates that the pole mass has an intrinsic uncertainty of order $\Lambda_{\rm QCD} \sim 200 - 300$ MeV. It is caused by the long range sensitivity of the pole mass and reflected in a factorial growth of the high order coefficients of the perturbation series connecting the pole mass to other mass definitions like $\overline{\rm MS}$ which seem to be free from this problem. Our results and the rather pessimistic prospect to further improve the results obtained in this paper certainly support this view. However, the notion of the renormalons might also give hints toward a more precise determination of the bottom quark mass because it implies that with a different mass definition the perturbative series for the moments might become better behaved. In this work we have not attempted to make use of this possibility, but we hope to return to this issue in the near future.

Acknowledgement

I am grateful to J. G. Branson, J. Kuti, Z. Ligeti, C. Morningstar, V. A. Sharma and J. J. Thaler for useful conversation. I thank A. V. Manohar for many helpful discussions and for reading the manuscript, and Z. Ligeti and M. B. Voloshin for their comments to the manuscript. This work is supported in part by the U.S. Department of Energy under contract No. DOE DE-FG03-90ER40546.

A NNLO Corrections from δH_{kin}, $V_{\rm BF}$ and $V_{\rm NA}$

In this appendix we present some details about the calculation of the NNLO corrections to the zero-distance Green function coming from the kinetic energy $\delta H_{kin}(\vec r) = -\vec\nabla^4/4M_b^3$, the Breit-Fermi potential $V_{\rm BF}$, Eq. (18), and the non-Abelian potential $V_{\rm NA}$, Eq. (21).

At NNLO the corrections coming from δH_{kin}, $V_{\rm BF}$ and $V_{\rm NA}$ are determined from first order time-independent perturbation theory,

$$[G_c^{(2)}(0,0,E)]^{\rm kin+BF+NA} \;=\; -\int d^3\vec r\, G_c^{(0)}(0,r,E)\,\delta H(\vec r)\, G_c^{(0)}(r,0,E)\,, \tag{109}$$

where

$$\delta H(\vec r) \;=\; -\frac{\vec\nabla^4}{4\,M_b^3} + V_{\rm BF}(\vec r) + V_{\rm NA}(\vec r)\,. \tag{110}$$

Because the zero-distance Green function only describes bottom-antibottom pairs in a ${}^3S_1$ triplet state, we can take the angular average and evaluate the spin operators for δH in expression (109). The form

of δH then simplifies to

$$\delta H_{3S1} \;=\; -\frac{\vec{\nabla}^4}{4\,M_b^3} - \frac{C_F\,a_s}{r}\,\frac{\vec{\nabla}^2}{M_b^2} + \frac{11}{3}\,\frac{C_F\,a_s\,\pi}{M_b^2}\,\delta^{(3)}(\vec{r}) - \frac{C_A\,C_F\,a_s^2}{2\,M_b\,r^2}\,. \tag{111}$$

Using the equation of motion for the Coulomb Green function, Eq. (26), we can eliminate the $\vec{\nabla}^2$ terms in δH_{3S1}. For illustration, let us consider the corrections coming from the term $-C_F\frac{a_s}{r}\frac{\vec{\nabla}^2}{M_b^2}$ in δH_{3S1}. Using the equation of motion we arrive at the relation

$$\begin{aligned}
&-\int d^3\vec{r}\,G_c^{(0)}(0,r,E)\,\Big[-\frac{C_F\,a_s}{r}\,\frac{\vec{\nabla}^2}{M_b^2}\Big]\,G_c^{(0)}(r,0,E)\\
&\quad=\;-\int d^3\vec{r}\,G_c^{(0)}(0,r,E)\,\Big[-\Big(\frac{C_F^2\,a_s^2}{M_b\,r^2}+\frac{C_F\,a_s}{r}\,\frac{E}{M_b}\Big)\,G_c^{(0)}(r,0,E)-\frac{C_F\,a_s}{M_b\,r}\,\delta^{(3)}(\vec{r})\Big]
\end{aligned} \tag{112}$$

The third term in the brackets represents a power divergence which is dropped in our convention (see the text after Eq. (30)). Using the same arguments for the kinetic energy term we get

$$\begin{aligned}
&-\int d^3\vec{r}\,G_c^{(0)}(0,r,E)\,\Big[-\frac{\vec{\nabla}^4}{4\,M_b^3}\Big]\,G_c^{(0)}(r,0,E) \qquad (113)\\
&\quad=\;\frac{E}{2\,M_b}\,G_c^{(0)}(0,0,E)-\int d^3\vec{r}\,G_c^{(0)}(0,r,E)\,\Big[-\frac{C_F^2\,a_s^2}{4\,M_b\,r^2}-\frac{E}{2\,M_b}\,\frac{C_F\,a_s}{r}-\frac{E^2}{4\,M_b}\Big]\,G_c^{(0)}(r,0,E)\,.
\end{aligned}$$

Collecting all terms from Eqs. (111)-(113) we arrive at

$$\begin{aligned}
&[G_c^{(2)}(0,0,E)]^{\rm kin+BF+NA}\\
&\quad=\;\frac{E}{2\,M_b}\,G_c^{(0)}(0,0,E)-\int d^3\vec{r}\,G_c^{(0)}(0,r,E)\,\Big[-\frac{E^2}{4\,M_b}-\frac{3\,E}{2\,M_b}\,\frac{C_F\,a_s}{r}\\
&\qquad+\frac{11}{3}\,\frac{C_F\,a_s\,\pi}{M_b^2}\,\delta^{(3)}(\vec{r})-\Big(\frac{5}{4}+\frac{C_A}{2\,C_F}\Big)\,\frac{C_F^2\,a_s^2}{M_b\,r^2}\Big]\,G_c^{(0)}(r,0,E)\,.
\end{aligned} \tag{114}$$

The first and the second term in the brackets on the RHS of Eq. (114) are handled by redefining the energy, $E \to E + E^2/4M_b^2$ and the coupling, $a_s \to a_s[1 + 3E/2M_b]$, in the nonrelativistic Coulomb Green function. The calculation of the δ-function term is trivial. The treatment of the $1/r^2$ term, on the other hand, is rather awkward. However, we can infer the correction caused the $1/r^2$ term by using the facts that the wave functions to the Schrödinger equation

$$\Big(-\frac{\vec{\nabla}^2}{m^2}-\frac{a}{r}-\frac{b}{m\,r^2}-E\Big)\,\Psi(\vec{r})\;=\;0 \tag{115}$$

can be determined exactly for any energy E (see e.g. Ref. [53]) and that the imaginary part of the Green function G of Eq. (115) in the continuum, i.e. for any positive energy E, is proportional to the modulus square of the scattering wave function at the energy E. From this it is straightforward to derive for positive energies the relation

$$\mathrm{Im}\,G(0,0,E)\;=\;\lim_{r\to 0}\,\Big[\,(2\,p\,r)^s\,\Big]\,\frac{m\,p}{4\,\pi}\,\exp\Big\{\,\frac{a\,\pi\,m}{2\,p}\,\Big\}\,\Big|\,\frac{\Gamma(1+s-i\frac{a\,m}{2\,p})}{\Gamma(2\,s+2)}\,\Big|^2\,, \tag{116}$$

where $s(s+1) = -b$ and $p = \sqrt{m(E+i\epsilon)}$. Expanding the RHS of Eq. (116) in small b[12] and imposing the short-distance cutoff $\mu_{\rm fac}$ as described in Section 3.1 we obtain for positive energies the relation

$$\mathrm{Im}\left[\int d^3\vec{r}\, G_c^{(0)}(0,r,E)\left(\frac{C_F^2\,a_s^2}{M_b\,r^2}\right)G_c^{(0)}(r,0,E)\right] \;=\; \frac{4\,C_F\,a_s\,\pi}{M_b^2}\,\mathrm{Im}\left[\left(G_c^{(0)}(0,0,E)\right)^2\right]. \qquad (117)$$

Due to analyticity relation (117) is then also valid for any real energy. Up to (irrelevant) constants we can therefore write

$$\int d^3\vec{r}\, G_c^{(0)}(0,r,E)\left(\frac{C_F^2\,a_s^2}{M_b\,r^2}\right)G_c^{(0)}(r,0,E) \;=\; \frac{4\,C_F\,a_s\,\pi}{M_b^2}\left[G_c^{(0)}(0,0,E)\right]^2. \qquad (118)$$

Collecting all terms the final result for the sum of the zero-distance Coulomb Green function and the NNLO corrections caused by δH_{kin}, $V_{\rm BF}$ and $V_{\rm NA}$ reads

$$\begin{aligned}
&G_c^{(0)}(0,0,E,a_s) + [G_c^{(2)}(0,0,E)]^{\rm kin+BF+NA} \\
&= \left(1+\frac{E}{2\,M_b}\right)G_c^{(0)}\Big(0,0,E+\frac{E^2}{4\,M_b},a_s\left[1+\frac{3\,E}{2\,M_b}\right]\Big) \\
&\quad +\frac{4}{3}\left(1+\frac{3\,C_A}{2\,C_F}\right)\frac{C_F\,a_s\,\pi}{M_b^2}\left[G_c^{(0)}(0,0,E,a_s)\right]^2
\end{aligned} \qquad (119)$$

up to corrections beyond the NNLO level. $G_c^{(0)}(0,0,E,a_s)$ is defined as the expression on the RHS of Eq. (31). Rewriting the energy in terms of $v = \sqrt{(E+i\epsilon)/M_b}$ we arrive at the result displayed in Eq. (36).

We do not want to leave unmentioned that for the treatment of the singular $1/r^2$ potential we have ignored the fact that its coefficient (mainly through the large non-Abelian contribution) is large enough that the $b\bar{b}$ system can collapse to a point (see e.g. [53]). This would lead to the breakdown of hermiticity. Thus, the result in Eq. (119) has some heuristic character. However, we strictly treat the singular $1/r^2$ (and also the $\delta^{(3)}(\vec{r})$) potential as a "small" perturbation to the Coulomb exchange and remove the arising UV singularities through the matching procedure. No exact treatment of the singular potential is intended. In this sense the result in Eq. (119) should be fine.

B Inverse Laplace Transforms

In this appendix we present the list of inverse Laplace transforms used to the calculate the theoretical moments at NNLO. In the following we use the conventions

$$\begin{aligned}
\Psi(z) &= \frac{d\ln\Gamma(z)}{dz}\,, \\
\Psi^{(n)}(z) &= \frac{d^n}{dz^n}\,\Psi(z)\,, \\
\Psi'(z) &= \Psi^{(1)}(z)\,,
\end{aligned}$$

[12] Because we want to treat the $1/r^2$ potential as a perturbation, the limit $r \to 0$ has to be taken after the expansion in b.

$$
\begin{aligned}
\Psi''(z) &= \Psi^{(2)}(z)\,, \\
{}_0F_2(a,b;z) &= \Gamma(a)\,\Gamma(b)\,\sum_{k=0}^{\infty}\frac{1}{\Gamma(a+k)\,\Gamma(b+k)}\,\frac{z^k}{k!}\,.
\end{aligned}
$$

$$
\frac{1}{2\pi i}\int\limits_{\gamma-i\infty}^{\gamma+i\infty}\frac{1}{x^\nu}\,e^{x\,t}\,dx = \frac{t^{\nu-1}}{\Gamma(\nu)}\,, \tag{120}
$$

$$
\frac{1}{2\pi i}\int\limits_{\gamma-i\infty}^{\gamma+i\infty}\frac{\ln x}{x^\nu}\,e^{x\,t}\,dx = \frac{t^{\nu-1}}{\Gamma(\nu)}\,\Big[\,\Psi(\nu)-\ln t\,\Big]\,, \tag{121}
$$

$$
\frac{1}{2\pi i}\int\limits_{\gamma-i\infty}^{\gamma+i\infty}\frac{\ln^2 x}{x^\nu}\,e^{x\,t}\,dx = \frac{t^{\nu-1}}{\Gamma(\nu)}\,\Big\{\,\Big[\,\Psi(\nu)-\ln t\,\Big]^2-\Psi'(\nu)\,\Big\}\,, \tag{122}
$$

$$
\frac{1}{2\pi i}\int\limits_{\gamma-i\infty}^{\gamma+i\infty}\frac{\ln^3 x}{x^\nu}\,e^{x\,t}\,dx = \frac{t^{\nu-1}}{\Gamma(\nu)}\,\Big\{\,\Big[\,\Psi(\nu)-\ln t\,\Big]^3-3\,\Big[\,\Psi(\nu)-\ln t\,\Big]\,\Psi'(\nu)+\Psi''(\nu)\,\Big\}\,, \tag{123}
$$

$$
\frac{1}{2\pi i}\int\limits_{\gamma-i\infty}^{\gamma+i\infty}\frac{1}{x^\nu}\,\sin(\frac{a}{\sqrt{x}})\,e^{x\,t}\,dx = \frac{a\,t^{\nu-\frac{1}{2}}}{\Gamma(\nu+\frac{1}{2})}\,{}_0\mathrm{F}_2\Big(\frac{3}{2},\nu+\frac{1}{2},-\frac{\mathrm{a}^2}{4}\,\mathrm{t}\Big)\,, \tag{124}
$$

$$
\begin{aligned}
\frac{1}{2\pi i}\int\limits_{\gamma-i\infty}^{\gamma+i\infty}\frac{\ln x}{x^\nu}\,\sin(\frac{a}{\sqrt{x}})\,e^{x\,t}\,dx &= \frac{a\,t^{\nu-\frac{1}{2}}}{\Gamma(\nu+\frac{1}{2})}\,\Big\{\,\Big[\,\Psi\Big(\nu+\frac{1}{2}\Big)-\ln t\,\Big]\,{}_0\mathrm{F}_2\Big(\frac{3}{2},\nu+\frac{1}{2},-\frac{\mathrm{a}^2}{4}\,\mathrm{t}\Big) \\
&\quad -\frac{d}{d\nu}\,{}_0\mathrm{F}_2\Big(\frac{3}{2},\nu+\frac{1}{2},-\frac{\mathrm{a}^2}{4}\,\mathrm{t}\Big)\,\Big\}\,,
\end{aligned} \tag{125}
$$

$$
\begin{aligned}
\frac{1}{2\pi i}\int\limits_{\gamma-i\infty}^{\gamma+i\infty}\frac{\ln^2 x}{x^\nu}\,\sin(\frac{a}{\sqrt{x}})\,e^{x\,t}\,dx &= \frac{a\,t^{\nu-\frac{1}{2}}}{\Gamma(\nu+\frac{1}{2})}\Big\{\Big[\Big(\Psi\Big(\nu+\frac{1}{2}\Big)-\ln t\Big)^2-\Psi'\Big(\nu+\frac{1}{2}\Big)\Big]\,{}_0\mathrm{F}_2\Big(\frac{3}{2},\nu+\frac{1}{2},-\frac{\mathrm{a}^2}{4}\mathrm{t}\Big) \\
&\quad -2\,\Big[\,\Psi\Big(\nu+\frac{1}{2}\Big)-\ln t\,\Big]\,\frac{d}{d\nu}\,{}_0\mathrm{F}_2\Big(\frac{3}{2},\nu+\frac{1}{2},-\frac{\mathrm{a}^2}{4}\,\mathrm{t}\Big) \\
&\quad +\frac{d^2}{d\nu^2}\,{}_0\mathrm{F}_2\Big(\frac{3}{2},\nu+\frac{1}{2},-\frac{\mathrm{a}^2}{4}\,\mathrm{t}\Big)\,\Big\}\,.
\end{aligned} \tag{126}
$$

C The Constants $w_p^{0,1,2}$ and $\tilde{w}_p^{0,1,2}$

In this appendix the constants $w_p^{0,1,2}$ and $\tilde{w}_p^{0,1,2}$ from expression (57) are given. They generically parameterize the higher order contributions to the Green function of the Schrödinger equation (24) coming from the radiative corrections to the Coulomb potential, $V_c^{(1)}$ and $V_c^{(2)}$, Eqs. (19) and (22). For

the constants $w_p^{0,1,2}$ we were able to calculate analytic expressions. The results read ($p = 1, 2, 3, \ldots$)

$$w_p^0 = -\frac{1}{p!\,\Gamma(\frac{p}{2})} \int\limits_0^\infty dt \int\limits_0^\infty du\, \frac{1}{(1+t+u)^2}\, \ln^p\Big(\frac{(1+t)\,(1+u)}{t\,u}\Big) = -\frac{(p+1)\,\zeta_{p+1}}{\Gamma(\frac{p}{2})}\,, \tag{127}$$

$$\begin{aligned} w_p^1 &= \frac{1}{p!\,\Gamma(\frac{p}{2})} \int\limits_0^\infty dt \int\limits_0^\infty du\, \frac{1-\ln(1+t+u)}{(1+t+u)^2}\, \ln^p\Big(\frac{(1+t)\,(1+u)}{t\,u}\Big) \\ &= -\Big\{ \frac{(1+p)}{\Gamma(\frac{p}{2})} \Big[\gamma_{\rm E}\,\zeta_{p+1} + \sum_{m=0}^\infty \frac{\Psi(2+m)}{(1+m)^{p+1}} \Big] + \frac{2}{\Gamma(\frac{p}{2})} \sum_{l=0}^{p-1} \sum_{m=0}^\infty (-1)^{p-l}\, \frac{(1+l)\,\Psi^{(p-l)}(2+m)}{(p-l)!\,(1+m)^{1+l}} \Big\} \end{aligned} \tag{128}$$

$$\begin{aligned} w_p^2 &= \frac{1}{p!\,\Gamma(\frac{p}{2})} \int\limits_0^\infty dt \int\limits_0^\infty du\, \frac{\zeta_2 - 2\,\ln(1+t+u) + \ln^2(1+t+u)}{(1+t+u)^2}\, \ln^p\Big(\frac{(1+t)\,(1+u)}{t\,u}\Big) \\ &= \frac{(1+p)}{\Gamma(\frac{p}{2})} \Big\{ \Big(\gamma_{\rm E}^2 + 2\,\zeta_2\Big)\,\zeta_{1+p} + \sum_{m=0}^\infty \frac{1}{(1+m)^{1+p}} \Big[2\,\gamma_{\rm E}\,\Psi(2+m) - \Psi'(2+m) + \Big(\Psi(2+m)\Big)^2 \Big] \Big\} \\ &\quad + \frac{2}{\Gamma(\frac{p}{2})} \sum_{m=0}^\infty \sum_{l=0}^{p-1} \frac{(-1)^{p-l}\,(1+l)}{(p-l)!\,(1+m)^{1+l}} \Big[2\,\gamma_{\rm E}\,\Psi^{(p-l)}(2+m) - \Psi^{(p-l+1)}(2+m) \\ &\qquad\qquad + 2\,\Psi^{(p-l)}(2+m)\,\Psi(2+m) \Big] \\ &\quad + \frac{4}{\Gamma(\frac{p}{2})} \sum_{m=0}^\infty \sum_{l=0}^{p-2} \sum_{k=1}^{p-l-1} (-1)^{p-l}\, \frac{(1+l)\,\Psi^{(p-l-k)}(2+m)\,\Psi^{(k)}(2+m)}{(p-l-k)!\,k!\,(1+m)^{1+l}}\,. \end{aligned} \tag{129}$$

The constants $\tilde{w}_p^{0,1,2}$ are calculated numerically. The corresponding integrals are ($i = 0, 1, 2$)

$$\tilde{w}_p^i = \frac{1}{p!\,\Gamma(\frac{p+1}{2})} \int\limits_0^\infty dt \int\limits_0^\infty du \int\limits_0^\infty dv \int\limits_0^1 ds\; \omega^i(t,u,v,s)\; \ln^p\Big(\frac{(1+t)\,(1+u)\,(1+v)\,(1-s)}{t\,u\,v\,s} \Big)\,, \tag{130}$$

where

$$\omega^0(t,u,v,s) = \frac{3\,x+y}{x^2\,(x+y)^3}\,, \tag{131}$$

$$\omega^1(t,u,v,s) = \frac{x^2 - 7\,x\,y - 2\,y^2}{x^2\,y\,(x+y)^3} + \frac{\ln x}{x^2\,y^2} + \frac{(y-x)\,(x^2+4\,x\,y+y^2)\,\ln(x+y)}{x^2\,y^2\,(x+y)^3}\,, \tag{132}$$

$$\begin{aligned} \omega^2(t,u,v,s) &= \frac{3\,x+y}{x^2\,(x+y)^3} - \frac{x+3\,y}{y^2\,(x+y)^3}\,\zeta_2 + \frac{(x-y)\,(x^2+5\,x\,y+y^2)}{x^2\,y^2\,(x+y)^3}\,\ln(x+y) \\ &\quad + \frac{3\,x+y}{x^2\,(x+y)^3}\,\ln^2(x+y) \\ &\quad - \frac{1}{x^2\,y^2}\Big[\ln x - \Big(\ln x - \ln(x+y)\Big)\,\ln y + {\rm Li}_2\Big(\frac{x}{x+y}\Big) \Big]\,, \end{aligned} \tag{133}$$

and

$$\begin{aligned} x &= 1 + t + u\,, \\ y &= 1 + v - s\,. \end{aligned}$$

References

[1] W. J. Stirling, Univ. of Durham Report No. DTP-97-80, hep-ph/9709429.

[2] M.B. Voloshin, *Int. J. Mod. Phys.* **A 10** (1995) 2865.

[3] M. Jamin and A. Pich, *Nucl. Phys.* **B 507** (1997) 334.

[4] J. H. Kühn, A. A. Penin, and A. A. Pivovarov, Univ. of Karlsruhe Report No. TTP98-01, hep-ph/9801356.

[5] V.A. Novikov *et al.*, *Phys. Reports* **41** (1978) 1.

[6] M. B. Voloshin and Yu. M. Zaĭtsev, *Usp. Fiz. Nauk* **152** (1987) 361 [*Sov. Phys. Usp.***30** (1987) 7].

[7] A. H. Hoang, *Phys. Rev.* **D 56** (1997) 5851.

[8] A. H. Hoang, proceedings of the "Workshop on Physics at the First Muon Collider and the Front End of a Muon Collider", Fermilab, November 6–9, 1997, hep-ph/9801273.

[9] A. H. Hoang and T. Teubner, UCSD Report No. UCSD-PTH 98-01, hep-ph/9801397.

[10] K. Melnikov and A. Yelkhovkii, Univ. of Karlsruhe Report No. TTP98-10, hep-ph/9802379.

[11] W. E. Caswell and G. E. Lepage, *Phys. Lett.* **B 167** (1986) 437.

[12] G. T. Bodwin, E. Braaten, and G. P. Lepage, *Phys. Rev.* **D 51** (1995) 1125.

[13] L. J. Reinders, H. R. Rubinstein, and S. Yazaki, *Nucl. Phys.* **B 186** (1981) 109.

[14] E. C. Poggio, H. R. Quinn, and S. Weinberg, *Phys. Rev.* **D 13** (1976) 1958.

[15] M. A. Shifman, A. I. Vainshtein, and V. I. Zakharov, *Nucl. Phys.* **B 147** (1979) 385; *Nucl. Phys.* **B 147** (1979) 448.

[16] A. H. Hoang, *Phys. Rev.* **D 57** (1998) 1615.

[17] W. E. Caswell, R. R. Horgan, and G. P. Lepage, *Phys. Rev.* **A 18** (1978) 810.

[18] A. H. Hoang, P. Labelle, and S. M. Zebarjad. *Phys. Rev. Lett.* **79** (1997) 3387.

[19] M. B. Voloshin, *Nucl. Phys.* **B 154** (1979) 365.

[20] E.H. Wichmann and C.H. Woo, *J. Math. Phys.* **2** (1961) 178.

[21] L. Hostler, *J. Math. Phys.* **5** (1964) 591.

[22] J. Schwinger, *J. Math. Phys.* **5** (1964) 1606.

[23] W. Fischler, *Nucl. Phys.* **B 129** (1977) 157.

[24] A. Billoire, *Phys. Lett.* **B 92** (1980) 343.

[25] S. N. Gupta and S. F. Radford, *Phys. Rev.* **D 24** (1981) 2309, *ibid.* **25** (1982) 3430 (Erratum); S. N. Gupta, S. F. Radford, and W. W. Repko, *Phys. Rev.* **D 26** (1982) 3305.

[26] M. Peter, *Phys. Rev. Lett.* **78** (1997) 602, *Nucl. Phys.* **B 501** (1997) 471.

[27] M. Abramowitz and I.A. Stegun, eds., *Handbook of Mathematical Functions* (Dover Publications, Inc., New York, 1972).

[28] I.S. Gradshteyn and I. M. Ryzhik, *Table of Integrals, Series and Products*, (Academic Press, Inc., San Diego, 1994).

[29] M.A. Braun, *Zh. Eksp. Teor. Fiz.* **54** (1968) 1220 [*Sov. Phys. LETP* **27** (1968) 652].

[30] G. Källen and A. Sabry, *K. Dan. Vidensk. Selsk. Mat.-Fys. Medd.* **29** (1955) No. 17.

[31] J. Schwinger, *Particles, Sources and Fields*, Vol II, (Addison-Wesley, New York, 1973).

[32] A. H. Hoang, *Phys. Rev.* **D 56** (1997) 7276.

[33] G. Adkins, R. N. Fell, and P. M. Mitrikov, *Phys. Rev. Lett.* **79** (1997) 3383.

[34] A. Czarnecki and K. Melnikov, *Phys. Rev. Lett.* **80** (1998) 2531.

[35] M. Beneke and V. A. Smirnov, CERN Report No. CERN-TH-97-315, hep-ph/9711391; M. Beneke, A. Signer, and V. A. Smirnov, *Phys. Rev. Lett.* **80** (1998) 2535.

[36] A. H. Hoang, J. H. Kühn, and T. Teubner, *Nucl. Phys.* **B 452** (1995) 173.

[37] S.G. Karshenboĭm, *Yad. Fiz.* **56** (1993) 155.

[38] R. Karplus and A. Klein, *Phys. Rev.* **87** (1952) 848.

[39] R. Barbieri *et al.*, *Phys. Lett.* **B 57** (1975) 455.

[40] K. G. Chetyrkin, J. H. Kühn, and M. Steinhauser, *Phys. Lett.* **B 371** (1996) 93; *Nucl. Phys.* **B 482** (1996) 213.

[41] K. G. Chetyrkin, J. H. Kühn, and A. Kwiatkowski, *Phys. Reports* **277** (1996) 189.

[42] K. G. Chetyrkin *et al.*, *Eur. Phys. J. C* **2** (1998) 137.

[43] H. Albrecht *et al*, *Z. Phys.* **C 65** (1995) 619.

[44] Particle Data Group, R. M. Barnett *et al.*, *Phys. Rev.* **D 54** (1996) 77.

[45] A. J. Buras, proceedings of the "Symposium of Heavy Flavours", Santa Barbara, July 7–11, 1997, hep-ph/9711217.

[46] *The BaBar Physics Book*, SLAC Report No. SLAC-R-504, in preparation.

[47] N. Gray *et al*, *Z. Phys.* **C 48** (1990) 673.

[48] DELPHI Collaboration, P. Abreu *et al.*, CERN Report No. CERN-PPE-97-141.

[49] W. Bernreuther, A. Brandenburg, and P. Uwer, *Phys. Rev. Lett.* **79** (1997) 189;
G. Rodrigo, M. Bilenky ,and A. Santamaria, *Phys. Rev. Lett.* **79** (1997) 193;
P. Narison and C. Oleari, *Phys. Lett.* **B 407** (1997) 57.

[50] S. J. Brodsky, G. P. Lepage, and P. B. Mackenzie, *Phys. Rev.* **D 28** (1983) 228.

[51] A. A. Penin and A. A. Pivovarov, Univ. of Karlsruhe Report No. TTP98-13, hep-ph/9803363.

[52] M. Beneke and V. M. Braun, *Nucl. Phys.* **B 426** (1994) 301;
I. I. Bigi, *Phys. Rev.* **D 50** (1994) 2234.

[53] L. D. Landau and E. M. Lifschitz, *Quantum Mechanics Vol.3*, (Butterworth-Heinemann, 1981).